AD NUMBER
AD363299
CLASSIFICATION CHANGES
TO: **UNCLASSIFIED**
FROM: **CONFIDENTIAL**
LIMITATION CHANGES
TO: **Approved for public release; distribution is unlimited.**
FROM: **Distribution authorized to U.S. Gov't. agencies and their contractors; Administrative/Operational Use; APR 1965. Other requests shall be referred to Office of Naval Research, Arlington, VA 22203.**
AUTHORITY
ONR ltr 4 May 1977 ; ONR ltr 4 May 1977

SECURITY MARKING

The classified or limited status of this report applies to each page, unless otherwise marked.
Separate page printouts MUST be marked accordingly.

"This document contains information affecting the National Defense of the United States within the meaning of the Espionage Laws, Title 18, U. S. C., Section 793 and 794. Its transmission or the revelation of its contents in any manner to an unauthorized person is prohibited by law."

DOWNGRADED AT 3 YEAR INTERVALS:
DECLASSIFIED AFTER 12 YEARS
DOD DIR 5200.10

" ONE HALF ORIGINAL SIZE "

attachment A

CONFIDENTIAL

MC-61-6-R3

RAIN EROSION ON SPIKE-PROTECTED SUPERSONIC RADOMES

(UNCLASSIFIED TITLE)

BY

JAMES E. NICHOLSON
JACQUES A. F. HILL

INTERIM ENGINEERING REPORT

APRIL 1965

MITHRAS, INC.
AEROTHERMODYNAMICS – ELECTROMAGNETICS – QUANTUM PHYSICS

701 CONCORD AVENUE, CAMBRIDGE, MASS. 02138

CONFIDENTIAL

CONFIDENTIAL

MITHRAS, INC.
701 Concord Avenue
Cambridge, Massachusetts
02138

MC-61-6-R3

RAIN EROSION ON SPIKE-PROTECTED SUPERSONIC RADOMES

(Unclassified Title)

by

James E. Nicholson

and

Jacques A. F. Hill

Interim Engineering Report

April 1965

This report contains viii and
83 pages. Copy No. [redacted]
MS Log 1534.

CONFIDENTIAL

FOREWORD

The research reported herein has been directed toward a study of the problem of rain erosion on radomes of high speed vehicles. During this year's research effort full scale sled test experiments of a solution to the rain erosion problem were successfully flown through rain at supersonic speeds. Scaling laws for rain erosion suppression were developed from a shock tube program on raindrop breakup.

This research was sponsored by the Department of the Navy's Office of Naval Research and Bureau of Naval Weapons under Contract Nonr 3684(00).

Scientific Officer for ONR Air Programs was Cmdr. Milton N. Gussow, and for BuWeps Missile Division, Mr. James M. Lee assisted by Mr. John Wright.

This report covers our third year's activity from October 1963, to October 1964.

The sled test series was conducted by the U. S. Naval Ordnance Laboratory (NOL) at Corona, California, with configurations specified by MITHRAS.

MITHRAS wishes to express its appreciation to NOL, Corona, for their cooperation during the sled test program. Appreciation is due to the Massachusetts Institute of Technology Aeroelastic and Structures Research Laboratory for their excellent support in the experimental shock tube program.

ABSTRACT

This report describes a sled test and shock tube test program designed to assess the effectiveness of flow separation devices in providing rain erosion protection to missile radomes. In the sled test program models were run at supersonic speeds through heavy rain. Those models with the flow separating device sustained little or no damage whereas unprotected models were totally destroyed by rain erosion. In the shock tube, drop breakup was studied over a wide range of the basic scaling parameters. Correlation of the shock tube data with previous drop breakup theory and extension of this theory to the sled test conditions yields results in excellent agreement. These results are then used to predict flow separation configurations at other altitudes and velocities of interest. Based on the results of these two experimental programs and the follow-up analysis, it may be concluded that flow separation techniques are an effective solution to the problem of rain erosion at supersonic speeds.

TABLE OF CONTENTS

Section			Page
	FOREWORD		ii
	ABSTRACT		iii
	LIST OF TABLES		vi
	LIST OF ILLUSTRATIONS		vii
1.	INTRODUCTION.		1
2.	SUMMARY AND CONCLUSIONS		3
3.	THE MECHANISM OF SPIKE PROTECTION AGAINST RAIN EROSION.		5
	3.1	The Rain Erosion Mechanism.	5
	3.2	The Spike-Induced Flow Pattern	7
	3.3	Interaction of Rain Drops with the Spike-Induced Flow Pattern	7
4.	DROP BREAKUP BY AIRSTREAM IMPACT		9
	4.1	Summary of Previous Investigations	9
	4.2	Modes of Drop Breakup.	13
	4.3	Scaling Laws for High-Speed Airstream Impact	14
5.	SHOCK TUBE MEASUREMENTS OF DROP BREAKUP.		17
	5.1	Description of the Experiment	17
	5.2	Criterion for Breakup Completion	18
	5.3	Results of the Shock-Tube Measurements.	19
6.	BREAKUP OF NATURAL RAIN BY THE SPIKE-INDUCED FLOW PATTERN.		21
	6.1	The Critical Drop Size	21
	6.2	Reduction of Water Impact on the Radome.	23

TABLE OF CONTENTS (Continued)

Section			Page
7.		SLED TESTS OF SPIKE-PROTECTED RADOMES	25
	7.1	Simulation of Natural Rain	26
	7.2	Description of the Tests	26
	7.3	Results Obtained on the 4-Inch Radome	27
	7.3.1	Unprotected Radome at 3000 ft/sec	27
	7.3.2	Spike-Protected Radome at 3000 ft/sec.	28
	7.3.3	Spike-Protected Radome at Transonic Speeds	29
	7.4	Results on the 8-Inch Radome.	30
	7.5	Measurements of Cut-Off Drop Size with the Spike Protected Faceplate.	31
	7.6	Correlation of the Sled Tests with the Shock Tube Measurements.	32
8.		PREDICTION OF SPIKE-PROTECTED RADOME PERFORMANCE IN FLIGHT.	34
	8.1	The Permissible Water Impact	34
	8.2	Flight Performance Versus Altitude and Radome Diameter.	36
9.		REFERENCES	38
Appendix A.		DIMENSIONAL ANALYSIS OF DROP BREAK-UP BY AIRSTREAM IMPACT.	69
Appendix B.		THE DISTRIBUTION OF DROP SIZES IN NATURAL RAIN	73
	B.1	The (M-P) Distribution of Drop Sizes	73
	B.2	Variation of the Mean Drop Diameter With Rain Rate.	75
DISTRIBUTION LIST.			80

LIST OF TABLES

Table		Page
1.	Summary of Shock Tube Test Conditions.	40
2.	Sled Test Run Schedule	41

LIST OF ILLUSTRATIONS

Figure		Page
1.	Spiked Induced Flow Pattern.	42
2.	Schematic of Drop Breakup by a Spike Induced Separated Flow	43
3.	Drop Distortion Model.	44
4.	Schematic of Shock Tube Experiment.	45
5a.	Dropmaker Apparatus.	46
5b.	Test Equipment.	47
6.	Sequential Photographs of Drop Breakup	48
7.	Drop Displacement and Velocity Versus Time.	49
8.	Summary Plot of Drop Breakup Time Versus Dynamic Pressure.	50
9.	Drop Displacement Versus Dynamic Pressure.	51
10.	Critical Drop Diameter d^* Versus Altitude.	52
11.	Effective (LWC) Versus Rain Rate for Several Values of Cut-Off Diameter	53
12.	Drawing of Sled Test Radome Geometry.	54
13.	Trackside Photograph of the Spiked Radome in the Rain Field.	55
14.	Unprotected 4-Inch Radome Before Firing-NO Spike	56
15.	Unprotected 4-Inch Radome After Firing-NO Spike	57
16.	Protected 4-Inch Radome Before Firing-with Spike	58
17.	Protected 4-Inch Radome After Firing-with Spike	59
18.	Post-Test Photograph of 4-Inch Transonic Model	60

LIST OF ILLUSTRATIONS (Continued)

Figure		Page
19.	Protected 8-Inch Radome After Firing-with Spike	61
20.	Post-Test Photograph of Spike Protected Flat Plate	62
21.	Flat Plate Surface Roughness Distribution . . .	63
22.	Allowable Rain Rate Versus Altitude for an 8-Inch Radome.	64
23.	Allowable Rain Rate Versus Altitude for a 12-Inch Radome.	65
24.	Allowable Rain Rate Versus Altitude for an 18-Inch Radome.	66
25.	Allowable Rain Rate Versus Radome Diameter for a Flight at 35000 Feet.	67
26.	Fraction of Time During Year That a Missile can Penetrate a Given Rainfall (New Orleans) . . .	68
B1.	Cumulative Volume Distribution with Drop Size .	77
B2.	Median Volume Diameter Versus Rain Rate . .	78
B3	Liquid Water Content Versus Drop Diameter for Several Rain Rates	79

1. INTRODUCTION

During the past three years, MITHRAS has been engaged in research leading to a solution to the rain erosion problem. Rain erosion is caused by the collision of raindrops with the leading edge of aircraft and missiles which fly at speeds in excess of 500 or 600 feet per second. Rather than seek materials of superior strength to withstand the raindrop impact, MITHRAS has investigated the possibility of using aerodynamic means of alleviating erosion damage. This solution consists of breaking up a major portion of the raindrops into harmless fog before the drops strike the aircraft or missile leading edge.

The aerodynamic device which has been studied for this purpose is a spike projecting into the relative wind ahead of the radome. This study is part of a general investigation of spike protected hemispherical radomes which has been carried out by MITHRAS for the U. S. Navy. The aerothermodynamic, mechanical and electromagnetic properties of this configuration have been studied, in addition to the protective features afforded by the spike against rain erosion. Some of the results of this research are reported in References 1 and 2.

The characteristic feature of the spike generated flow field is the conical region of separated flow extending from the tip of the spike to the face of the vehicle body. The radome is sized with respect to the body diameter so as to locate it entirely within this separated region. Thus it is subjected to a constant pressure environment whose temperature is also constant and may be controlled.

In an atmosphere-fixed coordinate system this whole separated region moves with the vehicle and raindrops encountering it are subjected to the impact of an airstream at the vehicle velocity. When raindrops are subjected to a step change in velocity, the droplet shape is distorted, and above some minimum velocity the drop breaks up into micron-size particles. The energy of each particle is considerably smaller than the original drop energy and the ratio of drag to mass for

this drop is increased in proportion to the inverse of the drop size. These particles are therefore rapidly accelerated and strike the radome with a relative velocity smaller than the vehicle speed. Both, because they are small and because their impact velocity is less, the damage caused by these fragments is much less than that which the original raindrops could inflict.

During 1961 and 1962 MITHRAS conducted wind tunnel test programs with a high velocity water injection gun to assess the effectiveness of spikes in affording rain erosion protection (Reference 1 and 2). Simulated rain was fired down the wind tunnel at several different models, simulating supersonic flight through the rain. Models protected with the spike-induced separated free layer received significantly less damage then unprotected models under similar rain and wind tunnel conditions. These experiments proved the feasibility of the spike configuration and provided a measurement of drop breakup distance for the specific wind tunnel test conditions. However, the wind tunnel test programs left unanswered two questions. They were:

1. What are the scaling laws for raindrop breakup by the impact of an airstream with various densities and velocities?

2. How can knowledge of the laws for drop breakup be used to obtain scaling laws for radome performance in flight through various intensities of rain at various speeds and altitudes?

The objective of the work reported here was to answer these two questions.

2. SUMMARY AND CONCLUSIONS

After examining the existing experimental data and available theoretical treatments, it was concluded that new measurements were required to define the breakup time of raindrops under the conditions corresponding to supersonic flight. The type of breakup under these conditions was identified and a simple scaling law was postulated. In order to confirm this law and to establish a value for the empirical constant which appears in it, a shock-tube test program was run. This test program was run in the MIT 8" x 24" shock tube over a wide range of airspeeds and densities. High speed photographic data was used to determine when drops are broken up. Observation of the instant of raindrop breakup was determined by noting a step change in acceleration of the water drop front. These data were correlated with the available drop breakup theory and with previous scattered measurements of drop breakup time and were found to be in excellent agreement. These results were used to predict drop breakup distances for drops of various sizes over a range of altitudes from sea-level to 70,000 feet.

Using a mathematical model of the drop-size distribution in natural rain, a simple model was devised to describe the reduction in water drop impact on the radome due to the breakup action of the spike induced flow pattern. Erosion was related to that portion of the liquid water content (LWC) of a rainfall with raindrops in excess of a certain cut-off diameter. This cut-off diameter was considered to be the limit size for a separation configuration which would cause rain erosion damage. It was related to the length of the dead-air region by means of a formula based on shock-tube measurements.

In order to obtain performance data on some complete configurations, several spike-protected radomes were run through simulated rain on the AFMDC Test Track at Holloman AFB, New Mexico. These tests were run by NOLC Corona on configurations specified by MITHRAS. Both 4-inch and 8-inch radomes were run at 3000 ft/sec though 6000 feet of simulated

rain falling at 5 inches/hour. This condition was severe enough so that an unprotected fiberglass radome was completely destroyed. On the other hand, both the 4-inch and 8-inch spike protected fiberglass radomes survived. Although there was appreciable surface erosion on the smaller dome, its structural integrity was maintained. Damage on the larger dome was confined to a number of isolated pits, which probably would not measurably degrade the performance of any radar using this radome. Another 4-inch spike-protected model was tested on transonic speeds through the same rainfall. It survived with a very few minor surface scars.

One sled test was run at 3000 ft/sec with a spike-protected aluminum disc. The distribution of surface roughness caused by rain erosion was measured and found to progress from minor pits near the center to severe roughness near the rim. This variation was related to the effective LWC which struck the plate near the center where the length of separated flow available for drop breakup was the greatest.

The results obtained in both test programs were combined to yield a prediction of spike performance in flight through natural rain at various speeds and altitudes. On the basis of these results the following conclusions may be drawn.

1. The use of a spike-generated flow pattern to break up rain drops and protect a radome against rain erosion is feasible. The intensity and extent of the rainfall through which a spike-protected radome may fly without damage decreases with altitude and flight speed and increases with radome size.

2. The performance of the spike-protected mechanism under various conditions may be predicted by the quantitative analysis developed herein.

3. Particularly on the larger missiles, with radome diameters of the order of 12 inches, the spike-induced reduction in water impact may be by as much as two orders of magnitude. Radome materials and shapes need not be chosen for their resistance to rain erosion and their electrical performance may be optimized. With spike protection it becomes entirely possible to use thin-walled spheres with low transmission losses.

3. THE MECHANISM OF SPIKE PROTECTION AGAINST RAIN EROSION

At supersonic speeds a spiked configuration creates a separated flow pattern which envelops a radome mounted within it. All but the largest rain drops are broken up before they can strike the radome. Both the unbroken drops and the fragments of the shattered ones are accelerated by the separated layer, achieving an appreciable fraction of the vehicle speed before striking the radome. Thus the energy of the drops incident upon the radome is considerably reduced by drop breakup and acceleration and the radome is eroded less severely.

3.1 The Rain Erosion Mechanism

Very little is actually known about the mechanism of material erosion by high-speed impact with raindrops. A voluminous literature exists on this subject but nearly all of it is of a qualitative, comparative nature (References 3 and 4). Nearly all of the experimental work, for instance, has consisted in comparing the resistance of various materials to some simulated rain environment.

It is certainly beyond the scope of this report to discuss in any fundamental way the mechanism of rain erosion, but some plausible, simple concepts are required in order to derive approximate scaling laws. We shall assume that the amount of material removed by the impact of any drop is proportional to the mass of the drop times some power of the normal velocity component relative to the surface. Actually there is a threshold below which the impact of a raindrop produces no permanent effect, but once this is crossed, and there is an erosion problem to consider, the generalization of projectile impact data is probably reasonably valid.

In the absence of any aerodynamic influence due to the flow field around the vehicle, the relative velocity of the drop is equal to the flight speed, V_∞, and the amount of erosion due to each drop is proportional to

$$\frac{\pi}{6} \rho d^3 V_\infty^n \cos\theta \qquad 3.1$$

In order to obtain the total amount of erosion incurred in flying through a rainstorm, this expression must be summed over all the drops encountered. These drops are of various sizes and it is convenient to introduce a drop-size distribution function N(d) which is the number of drops per unit volume and per unit diameter interval. The total number of drops per unit volume is

$$n = \int_0^\infty N(d)\, dd \qquad 3.2$$

The total erosion per unit area per distance flown is then

$$\frac{\pi}{6} \rho V_\infty^n \cos\theta \int_0^\infty N(d)\ d^3\ dd \qquad 3.3$$

which may be written

$$(LWC) \times V_\infty^n \cos\theta \qquad 3.4$$

where

$$(LWC) = \frac{\pi}{6} \rho \int_0^\infty N(d)\ d^3\ dd \qquad 3.5$$

is the liquid-water content of the air through which the vehicle is flying. (LWC) is expressed as a density with units of grams/meter^3.

This idealized analysis neglects the existence of the threshold values of V_∞ and d below which no damage occurs. It probably constitutes a reasonable approximation, however, for the larger velocities and drop sizes relevant to the rain erosion problem. It certainly represents an improvement over simply counting drops, since it does account for the fact that larger drops do more damage.

3.2 The Spike Induced Flow Pattern

The spike-induced flow pattern is shown schematically in Figure 1. The major feature of the flow field is the dead-air region which is bounded at the base by the body face and at the sides by a shear layer. This free shear layer begins where the boundary layer on the spike separates because of pressure rise at the dead-air region and ends at or near the edge of the body face where it re-attaches to form a conventional boundary layer. The velocities in the separated flow or dead-air region are very much smaller than in the free stream, and the pressure is nearly constant. Therefore, this region assumes a conical shape with the cone axis aligned with the flow. At the point of re-attachment, some of the boundary-layer air, with significant velocity, is turned into the separated region and causes the low-speed circulation in the region.

Because re-attachment of the free shear layer onto the radome itself would be undesirable, its diameter is deliberately made somewhat smaller than that of the front face of the missile. A discussion of the diameter ratio required has been given in Reference 1 and 2.

3.3 Interaction of Rain Drops with the Spike-Induced Flow Pattern

The spike-induced flow ahead of the radome subjects any raindrop it encounters to the impact of an airstream moving at the vehicle speed. As shown in Figure 2, this impact is actually applied in two steps, first at the shockwave and then at the mixing layer. The first impact is much smaller than the second. At moderate supersonic flight

speeds the airstream felt by a drop after the shockwave passes it is only about 10 percent of the vehicle speed. Only after the drop becomes immersed in the conical region of separated flow does it feel the full impact of an airstream moving at the flight speed of the vehicle.

This impulsively applied airstream has two effects on raindrops. Both effects greatly reduce the raindrop capability to erode the radome surface. In the first place the air stream will shatter most drops into much smaller droplets. In the second place it will accelerate both unshattered drops and drop fragments to some fraction of the vehicle velocity. This will reduce the relative velocity at impact and hence, by equation 3.1 the amount of erosion. Most easily accelerated will be the smaller drops and drop fragments. It is a reasonable hypothesis that none of the water originally present in drops can do any damage when shattered. As far as erosion damage is concerned, only the (LWC) of drops which are too large to be shattered need be counted. Even these drops are accelerated and lose some of their mass before impacting the radome, so that the damage they can do is less than if they impacted at the vehicle speed.

In order to develop this qualitative description into a quantitative one, detailed information is required on the breakup of drops by airstream impact and on the raindrop sizes encountered in rain of various intensities.

4. DROP BREAKUP BY AIRSTREAM IMPACT

When a liquid drop is suddenly exposed to an airstream, various competing forces act to determine whether it will be broken up and, if so, how long the process will take. The basic effect on the drop is a distribution of surface pressure loadings which scales approximately with the airstream dynamic pressure, $1/2\ \rho V^2$. The tendency of this pressure loading to distort the drop shape is resisted by inertia forces, surface tension forces, and, to a lesser extent, viscous forces.

Appendix A presents a dimensional analysis of the problem in which all the variables are considered and grouped into standard non-dimensional parameters. The most important of these for the following discussion is the Weber number.

$$We = \frac{\rho_g V^2 d}{2\sigma} \qquad 4.1$$

which represents the ratio of the pressure to surface tension forces. This parameter is the primary one for determining whether a drop will breakup at all. For airspeeds much larger than the minimum required for breakup, on the other hand, it loses its importance. In fact, under the conditions encountered in supersonic flight the breakup process is dominated by pressure and inertia forces, and several of the parameters obtained from the dimensional analysis of Appendix A may be ignored.

4.1 Summary of Previous Investigations

One of the earliest investigators of drop breakup was Lane, (Reference 5) who stated that there is a minimum step change in velocity required to break up drops. Lane's experiment consisted of a micro-burette mounted transverse to a shock tube. Drops varying in size from 500 to 5000 microns fell from a specially designed microburette past the center of the shock tube. The shock tube was fired by a signal from a

photocell which was triggered by the falling drop. By varying the strength of the shock front, it was possible to determine a critical velocity for drop breakup. These measurements were extended by Rupe, (Reference 6) who, using a microburette similar to Lane's, generated drop sizes as small as 75 microns in diameter.

Further measurements of drop breakup were made by Hanson, et al, (Reference 7) who suspended drops in the center of a shock tube by acoustical radiation pressure. A detailed description of the ultrasonic drop suspension systems is given in Reference 8. This device was capable of supporting drops ranging in size from 100 μ to 3000 μ at atmospheric pressure. In Hanson's experiment, precise measurements of the critical Weber number were obtained for both water and methyl drops over a range of impact velocities. In addition, high quality photographs of drop breakup were obtained for different values of the time delay measured from the arrival time of the shock front at the drops. For small step changes in the impact velocity (values of the Weber number close to $(We)_{crit}$, a blow-out process for drop breakup was observed. For step changes in the impact velocity corresponding to a Weber number approximately three times $(We)_{crit.}$, the drop breakup process was observed to be a stripping action. That is, the blow out type of drop breakup has been observed to exist only over a narrow range of Weber number. This effect has been confirmed recently by Clark, (Reference 9).

The early investigations by Lane and Hanson, et. al. were mainly concentrated in measuring the drop breakup process for small changes in the impact velocity. All data corresponded to subsonic flow aft of the shock front. Sufficient data had not been collected to substantiate any particular drop breakup theory.

One of the earliest studies of drop breakup in a shock tube for collision of drops with strong shocks was conducted by Engel, Reference 10. Shock front speeds corresponding to Mach numbers of 1.3, 1.5 and 1.7 were achieved. Drop breakup of 2.7 mm drops was studied in great detail for each of the above conditions. The observed phenomenon

consisted of several stages of breakup starting with an initial period of inactivity followed by an adjustment period in which the drop shape flattened out perpendicular to the direction of the airflow. This is followed by a period of approximately 120 μ seconds in which the drop size remains constant. After this period of inactivity and at a total time of about 300 μ seconds, drop breakup begins as material is stripped from the edge of the drop. This process continues until the drop is completely broken up.

While the investigation of the drop breakup process was extensive, results were obtained for only three conditions of the local flow. In Engel's experiment the driven pressure was maintained at one atmosphere. Consequently local flow conditions for the three shock speeds were fixed. Drop breakup was recorded by photographing the phenomenon at different time intervals after the shock arrival at the drop. For the low Mach number test, the final drop breakup time was not noted, except to observe that it was greater than 742 μ sec after the air-shock-waterdrop collision.

The experiment at Mach number 1.5 was extended in time to observe the final breakup of the 2.7 mm drop. After a time interval of 764 μ sec, the photograph obtained by Engel indicates that the drop is very close to being broken up. The dynamic pressure corresponding to the local conditions is 8.89 psia.

Additional experiments were conducted to determine breakup of 1.4 mm diameter waterdrops at Mach number 1.5. For the same dynamic pressure, photographs indicate that drop breakup occurred at a short time after 411 μ sec but prior to 492 μ secs.

Experiments of drop breakup of 2.7 mm-diameter waterdrops in a Mach number 1.7 flow indicated that drop breakup occurred at approximately 594 μ sec after shock collision with the drop.

While the above data were a substantial contribution in determining the drop breakup mechanism, data were obtained at only two values of the dynamic pressure. Assuming the waterdrop breakup equation derived by Gordon, (Reference 11), Figler (Reference 1) correlated Engel's results

and found agreement within 30 to 40 percent. Because there was no concrete breakup criterion established, part of the disagreement results from the inability to fix an experimental breakup time. The remainder of the disagreement is due to the inaccuracies of the available theory.

Other studies of drop breakup have been conducted by Figler, (References 1 and 2). In these investigations a high pressure water gun was designed and constructed to deliver a distribution of drops at a high velocity. This gun was mounted in a wind tunnel and fired downstream at speeds matched closely to the supersonic flow velocity. Cylindrical models were mounted in the test section with the geometrical axis aligned with the flow. No direct measurements were made of the drop breakup time. However, a quantitative measurement of drop breakup distance was obtained by varying the length of the dead air region until drops were broken up.

In the two experiments conducted in the MIT wind tunnel, Reference 1, and the David Taylor Model Basin wind tunnel, Reference 2, neither facility had the capability to change static pressure at the test section. Consequently it was not possible to determine the separate effects of velocity, Mach number and density ratio on the drop breakup length.

Recent work on the breakup of liquid jets by a transverse flow has been conducted by Clark, (Reference 9). In this experiment a continuous jet of water was injected into the path of a moving gas flow varying in velocity from 65 to 430 feet per second. The liquid velocity varied from 15 to 155 fps. Three different diameter jets were investigated: .065, .089 and .120 inches. Based on these conditions the Weber number was found to range from 31 to 11000. It was observed in Clark's experiment that drop breakup depends mainly on dynamic pressure of the moving gas with respect to the jet.

4.2 Modes of Drop Breakup

The results of the investigation described above allow us to distinguish three principal ways in which a liquid drop may be broken up by the impact of an airstream. These are:

1. The drop vibrates with an increasing amplitude until it breaks up.
2. The drop inflates like a parachute until it bursts in the center.
3. The drop flattens out to a disc and material is stripped from the radome edge.

The way in which breakup actually occurs in any given situation seems to depend mainly on the value of the Weber number. First of all, there is a critical value, $(We)_{crit}$, which must be exceeded before the drop can be broken up at all. For values of We only slightly larger than this critical value, the first model of breakup occurs. As We increases, there is a small range of value for which the drop inflates and bursts. Finally, for large values of We, breakup occurs by flattening and stripping.

The consensus of the previous investigation is that a value of We large enough to induce this last-named breakup process is not much larger than the critical value. In fact

$$We > 3\,(We)_{crit} \qquad 4.2$$

seems to be large enough. Values of $(We)_{crit}$ measured for water range from about 4 to 13. At sea-level, these correspond to velocities of 40 to 200 ft/sec for drop diameters in the 1 mm - 2 mm range which are most prevalent at the rain rates of interest. Obviously then, only the flattening and stripping type of breakup is relevant to a discussion of spiked configurations in high-speed flight. In this situation the inertia forces are many times larger than the surface-tension forces.

It may also be demonstrated that viscous effects may be neglected in the case of high-speed flight through rain. The Reynolds numbers

based on air properties, Re_a, are of the order of 100,000. In this range pressure drag on a sphere is much larger than the friction drag. As for viscous effects in the water, Gordon, (Reference 11) has shown that the ratio of the viscous retarding pressure to the impact pressure of the airstream is of the order of $32/Re_w$. Since

$$Re_w \approx 0.02\, Re_a \qquad 4.3$$

this viscous effect can also be neglected.

4.3 Scaling Laws for High-Speed Airstream Impact on Drops

Since the surface tension and viscous forces are much smaller than the pressure and inertia forces in the case of high-speed airstream impact on drops, the two Reynolds numbers and the Weber number need no longer be considered in the general breakup function of Appendix A. The dependence of breakup time on the parameters which remain relevant may be written

$$\bar{t}_b = \frac{t_b V}{d} = f'\left(\frac{\rho_\ell}{\rho_a} , M \right) \qquad 4.4$$

The Mach number, M, represents the influence of the compressibility of air. Its effect on $\bar{t}_b$ should be small for subsonic speeds. At transonic speeds it may begin to play a role through changes in the pressure distribution on the spherical drop. This pressure distribution again becomes invariant for $M > 2.5$ or so and no further Mach number dependence should be expected. Not enough data are available to substantiate these plausible conjectures and, subject to confirmation by the experiments described below, we shall assume that the Mach number of the impacting airstream plays a minor role in the drop breakup process.

The functional relation now remaining

$$\bar{t}_b = \frac{t_b V}{d} = f\left(\frac{\rho_\ell}{\rho_a}\right) \qquad 4.5$$

is simple enough so that an attempt to establish the form of the function seems worthwhile. For this purpose the drop breakup process may be described as sketched in Figure 3 which is based on Reference 9.

The rate of change of drop distortion, δ, (see Figure 3) is computed from Newton's third law

$$\ddot{\delta} = \frac{1}{\rho_\ell} \Delta p \qquad 4.6$$

where Δp is the pressure gradient transverse to the drop. Now the impact pressure is roughly $\rho_a V^2$ and is much larger than the pressure at the edges of the drop. Initially, therefore,

$$\Delta p \approx \frac{2\rho_a V^2}{d} \qquad 4.7$$

and

$$\ddot{\delta} = \frac{2\rho_a}{\rho_\ell} \frac{V^2}{d} \qquad 4.8$$

Neglecting, in this simple model, any changes in Δp as the drop distorts, the distortion as a function of time may be written

$$\delta = \frac{\rho_a}{\rho_\ell} \frac{V^2}{d} t^2 \qquad 4.9$$

The relative distortion is

$$\epsilon = \frac{\delta}{d} = \frac{\rho_g}{\rho_\ell} \left(\frac{Vt}{d}\right)^2 \qquad 4.10$$

Breakup is assumed to occur when ϵ reaches a critical value, to be determined by experiment.

In terms of aeronautical parameters this scaling law for high-speed breakup can be written

$$\frac{t_b}{d} = \left(\frac{\epsilon \rho_\ell}{2}\right)^{1/2} q^{-1/2} = k\, q^{-1/2} \qquad 4.11$$

where q is the impact dynamic pressure.

If

q is measured in psi

t_b in milliseconds

d in inches

then

$$k = 6.85 \sqrt{\epsilon} \qquad 4.12$$

5. SHOCK TUBE MEASUREMENTS OF DROP BREAKUP

In order to obtain definitive data on drop breakup under conditions relevant to high-speed flight through rain, a series of experiments were run in the MIT 8" x 24" shock tube. The objectives of these experiments were to confirm, if possible, the scaling laws for high-speed impact developed in the previous section and to obtain the value of the empirical constant in the formula (4.11). Before these objectives could be realized it was found necessary to establish an unambiguous definition of the completion of the breakup process so that the interval t_b could be measured. This point has been neglected by previous investigators whose interest lay mainly in low-speed impact and determination of $(We)_{crit}$.

5.1 Description of the Experiments

The shock tube in the Aeroelasticity and Structures Laboratory at MIT has been described elsewhere (Reference 12). It is driven by cold air or helium and is capable of generating airspeeds behind the shockwave up to about 3000 ft/sec. The initial pressure may be reduced to about 0.5 psia by vacuum pumps.

During these tests drops with a nominal diameter of 1.5 mm were introduced into the shock tube by dripping water from .016-inch hypodermic tubing mounted in the top of the shock tube. The firing of the shock tube was synchronized with the start of a Fastax camera which photographed the breakup process at about 13,000 frames per second. The arrival of the shock wave at the drop was determined by an event marker. Frame rate was measured with a 120 cps timing light. A schematic of the experimental setup is shown in Figure 4 and a photograph of the apparatus is given in Figure 5.

The test program consisted of 32 runs, covering the 6 test conditions listed in Table 1. Initially the camera covered a fairly small field of view in order to obtain enough magnification to allow a measurement of drop size. Later the same conditions were repeated with a large

field of view in order to follow the breakup process to completion.

A typical sequency of photographs obtained with the small field of view is shown in Figure 6. The individual frames have been aligned with a fixed reference mark in the shock tube so that they show the motion of the drop as well as its breakup as expected, these pictures indicate that the breakup process was of the third type discussed in section 4.2 above. The drops were first deformed into discs normal to the flow and then droplets were stripped from the exposed edges.

5.2 Criterion for Breakup Completion

Since the breakup of the drop proceeds by the stripping of smaller droplets from its edges, it is reasonable to call the process complete when the remaining drop is not much larger than the fragments which are being stripped off.

Since a steady light source was used to take the Fastax pictures, the exposure time was set by the camera framing rate and was much too long to resolve moving drops. However, an indication of the size of the shrinking drop may be obtained by examining its motion. (Its location is of course at the leading edge of the droplet cloud seen in the photographs). Figure 7 shows a curve of drop displacement versus time for a typical run. Also shown is a curve of drop velocity versus time obtained by numerical differentiation of the displacement data. The sharp break in the slope of the velocity curve was observed in every run. It indicates a sudden increase in the drop acceleration and hence in the area/volume ratio. Apparently at this point the remaining core of the original drop shatters into a number of much smaller drops. For practical purposes the breakup process is complete and a value of the breakup time, t_b, may be read off the curve.

This definition of t_b was adopted for all the data and values were read off curves similar to the one illustrated in Figure 7. It is a new definition and introduces a quantitative criterion for the completion of breakup where previous investigators had relied on subjective interpretation of photographs.

5.3 Results of the Shock-Tube Measurements

The data obtained in the shock-tube measurements have been plotted in Figure 8 in a manner suggested by the analysis of section 4.3, namely t_b versus the dynamic pressure, $q = \frac{1}{2} \rho_a V^2$. With logarithmic scales on both axes, the formula (4.11) is represented by a straight line with a slope of - 1/2. Such a line has been drawn and fits the data quite well.

The equation of the line shown may be written

$$t_b/d = 23.9\, q^{-1/2} \qquad 5.1$$

where t_b is the breakup time in milliseconds

d is the drop diameter in inches

q is the dynamic pressure in psia

The corresponding value of the empirical constant of section 4.3,

$$\epsilon = \frac{2q}{\rho_\ell} \left(\frac{t_b}{d}\right)^2 \qquad 5.2$$

is $\epsilon = 12$. This is in excellent agreement with the previously reported range of values between 10 and 15.

Some data from previous experiments have also been plotted in Figure 8. Quite good agreement with the present results is obtained in spite of possible differences in the definition of the completion of the breakup process.

The shock-tube results may also be used to define a breakup distance, that is the displacement of the drop during the breakup process. Figure 7 shows that the drop acceleration is approximately

constant during the breakup process, so that the displacement may be written

$$S_b = \frac{1}{2} \; a \; t_b^{\,2} \qquad 5.3$$

The acceleration, a, is equal to the ratio of the aerodynamic drag on the drop to its mass,

$$a = \frac{D}{m}$$

$$= \frac{3C_D}{4} \quad \frac{\rho_a V^2}{\rho_e d} \qquad 5.4$$

where C_D is the drag coefficient. Therefore

$$S_b = \frac{3C_D}{8} \quad \frac{\rho_a V^2}{\rho_e} \quad \frac{t_b^{\,2}}{d} \quad d$$

$$= \frac{3}{8} \epsilon \; C_D \; d \qquad 5.5$$

where ϵ is the empirical constant introduced in section 4.3. The drag coefficient C_D on the distorted drop is not known but may be presumed invariant. This simple analysis thus predicts that S/d should be constant.

Figure 9 shows the values of S/d measured in the shock-tube experiments versus the impact dynamic pressure. The predicted invariance is confirmed within the experimental accuracy and the best fit to the data is

$$S_b/d = 12 \qquad 5.6$$

Note that this value is independent of the velocity or density of the air (since only water drops were used, a possible variation with the density of the liquid cannot be ruled out).

6. BREAKUP OF NATURAL RAIN BY THE SPIKE-INDUCED FLOW FIELD

A qualitative discussion of the action of a spike-induced flow pattern on raindrops has been given in section 3.3. With the information we now have on the times and distances required to breakup rain drops of various sizes, we can make this discussion more quantitative. We still do not pretend to be able to predict from first principles the amount of rain erosion suffered by any particular configuration in flying through a given rainstorm. We can, however, compute what fraction of the total liquid water content of the rainfall is rendered harmless by the spike. These computations can then be used later to provide scaling laws. Tests under one particular condition of simulated rain can thus yield estimates of performance at other rain rates and altitudes.

6.1 The Critical Drop Size

When a spike-protected radome encounters rain consisting of a wide range of drop sizes, not all the drops will necessarily be broken up before striking the radome. The results of the previous section indicate that the distance required to break up a drop increases with the diameter of the drop; for a configuration of a given size, therefore, only drops whose diameter lies below a certain critical value will be broken up.

It was stated in section 3 that the airstream impact on the raindrop essentially starts when it crosses the mixing layer. Consider a station on the radome which lies a distance X (measured parallel to the flight path) behind the mixing layer. The critical drop for this station strikes the surface t_b milliseconds after encountering the mixing layer. During this time it has moved a distance S_D. In order to catch up with it the radome must travel a distance $X + S_D$ in the time t_b. Thus

$$V t_b = X_b + S_D \qquad 6.1$$

for this critical drop. Substitution of the formulas (5.1) and (5.6) for t_b and S_D yields for the diameter of the critical drop;

$$d^* = \frac{X}{\left[\left(\frac{\epsilon \rho_f}{\rho_a}\right)^{1/2} - 12\right]} \qquad 6.2$$

where ρ_a is the air density in the conical separated region.

Figure 10 gives values of the critical drop diameter d^* versus altitude for several values of the separation distance X. Since at any altitude d^* is proportional to X, interpolation for intermediate values of X is simple. The curves have been drawn for configurations with an effective cone angle of 20°, which has been used in several previous investigations and is just blunt enough to ensure separation at the spike tip for turbulent flow. Although the density in the formula (6.2) is that of the dead-air region, no Mach number effect is noted in plotting the results against altitude. For this cone angle it turns out that the pressure and temperature rises in going from the ambient to the dead-air region combine to give an essentially constant density ratio

$$\rho_a/\rho_\infty = 1.28 \qquad 6.3$$

over the Mach number range from shock detachment at M = 1.22 to hypersonic values.

Now for any radome-spike configuration, the separation distance X will vary along the radome surface. At the same time the angle of impact of the drops will vary and it is very difficult, in the absence of good models of rain erosion, to establish where on the radome erosion is likely to be the most severe. For the simple design sketched in Figure 12 it was found in the sled tests described below that the most severe damage occurred at the 45° station on the hemispherical radome.

At this point the ratio of the separation distance X to the radome diameter D, assuming a 20° cone angle, is

$$X/D = 0.74 \qquad 6.4$$

and the values of d^* corresponding to this location may be scaled from Figure 10. At sea-level, for instance this critical value of d^* is simply

$$d^* = .248\ D \qquad 6.5$$

if d^* is in mm and D is in inches.

6.2 Reduction of the (LWC) of Natural Rain Impacting on the Radomes

For a given specific radome-spike configuration the results presented in Figure 10 allow us to compute as a function of altitude the largest raindrops which will be broken up before striking the radome. All raindrops larger than the critical diameter d^* will strike the radome before the drops are completely broken up. Some of the drops, not much larger than the critical size, will have been stripped of most of their mass and will have been accelerated to some appreciable fraction of the vehicle velocity. These drops will do less damage to the radome than if they had not been acted upon by aerodynamic forces. Still larger drops will be less affected by aerodynamic impact in the breakup distance available, and they will impact on the radome with close to the full force.

It is clear from the above discussion that only that portion of the liquid-water-content which includes drops larger than a certain cut-off size are effective in producing rain erosion damage. This cut-off size is larger than the critical diameter d^* and depends on the particular radome material being used. In this idealized model we will consider only that portion of the (LWC) with drops of diameter acted upon by aerodynamic forces. Still larger drops will be less affected by aerodynamic impact in the distance available, and they will impact on the radome with close to the full force.

Only that portion of the liquid-water-content which includes drops larger than a certain cut-off size will be considered capable of causing rain erosion damage. The cut-off diameter d' is larger than the critical diameter d^* and depends in part on the erosion resistance of the radome. The cut-off diameter will be related to the critical diameter by

$$d' = \eta d^* \qquad 6.6$$

where η is an unspecified factor which is greater than one.

In order to compute the effect of a cut-off diameter d' on the (LWC) of a rainfall, it is necessary to know the drop-size distribution. The distribution generally used for meteorological calculations is given in Appendix B. In particular, Figure B.3 gives the volumetric distribution of drop sizes for a number of rain rates. Using these data, Figure 11 has been drawn. In it the effective (LWC) has been plotted versus the rain rate for several values of the cut-off diameter d'. For a given configuration flying at a given speed, the value of d' is fixed (and may be computed except for the factor η from the formulas given in this report). The amount of rain-erosion protection it provides corresponds to the displacement of the appropriate d' curve below the curve for the total (LWC).

Various scaling laws may be derived from the curves of Figure 11, as discussed below. We note here only that the value d' required to achieve a certain amount of protection, (say (LWC) one order of magnitude below the total) increases with the rain rate. This can be deduced directly from the figures presented with Appendix B. Figure B.1 shows that this degree of protection requires that

$$d' \approx 1.8\, d_o \qquad 6.7$$

where d_o is the median volume diameter which divides the rainfall into two equal volume fractions. In the empirical rainfall model derived from meteorlogical observations, d_o increases with the rain rate as illustrated in Figure B.2.

7. SLED TESTS OF SPIKE-PROTECTED RADOMES

Various techniques are available for testing spike-protected radomes in simulated rain. Figler (References 1 and 2) has used a wind tunnel with a high-speed water gun in an earlier phase of the MITHRAS program. In the transonic speed regime the whirling-arm technique may be used. In order to obtain data over a range of speeds from 3000 ft/sec down through the transonic range a sled-test facility was used during this phase of the MITHRAS program.

A series of six sled test runs were conducted at the high-speed rain erosion test track at the Air Force Missile Development Center Test Track Division at Holloman Air Force Base, New Mexico (Reference 13). Configurations for the six runs were supplied by MITHRAS to the Naval Ordnance Laboratory, (NOLC) Corona, California which directed the test for the Navy.

The high-speed track at Holloman is 35,000 feet long with a 6000 ft run of simulated rain. Rain is generated by mounting precisely controlled nozzles in a double row along the test track. The rain rate was 5 inches per hour with a nominal drop size of 1.5 mm.

Of the six sled test runs, five were run at supersonic speeds ranging from 2830 feet per second to 3050 feet per second. The sixth run was transonic ranging from 1450 feet per second to 765 feet per second. The velocity of the supersonic sled test vehicles were attained by two stages of Genie propulsion and then sustained by a 2.2 KS 11,000 sustainer engine. The variation of velocity through the rain field was less than 100 fps between entry to and exit from the rain field. The velocity of the transonic sled was attained by a 2.2 KS 11,000 sustainer engine. No thrust was applied during the rain field traverse for the transonic run.

7.1 Simulation of Natural Rain

Rain erosion investigations carried out on rocket-sled tracks are generally in the nature of proof tests of one material against another and a close simulation of natural rainfall is not attempted. Since the length of track available is limited, a very intense rainfall is used to simulate flight for a much longer distance through the less intense rainfall likely to be encountered operationally. This concept is consistent with the simple rain erosion formulas discussed in section 3.1 above, especially if the scaling is done in terms of (LWC) rather than the rain rate.

Not much information is available about the drop sizes of the simulated rain at the Holloman Air Force Base except that the mean drop diameter for our tests was about 1.5 mm. The kind of mean is not defined. A median volume diameter of 1.5 mm corresponds to a rain rate of about 0.5 in/hr. (see Figure B.2). In terms of this measure of drop size the 6000 feet of artitical rain falling at 5 in/hr is quite simulation of 60,000 feet of rain falling at 0.5 in/hr. Nothing is known, however, about the simulation of drop size distribution, which plays a very important role in determining the effectiveness of a spike-protected configuration. In any future tests, it is hoped that this characteristics of the artifical rain can be measured.

7.2 Description of the Experiments

A run schedule of the 6 tests is given in Table 2. This gives the velocities at rain field entry and exit. The basic configuration consisted of a 4-inch diameter fiberglass radome, 1/4 inch thick, mounted on a 6-inch faceplate. The spike was mounted on the same faceplate and simply protruded through a hole in the radome. It was 7 inches long and thus protruded 5 inches upstream of the radome. A drawing of this model, which was used in three of the six runs, is shown in Figure 12. A similar model scaled up by a factor of two in every dimension, (except wall thickness, which remained 1/4 inch) was run once. As a tare run the

4-inch radome was also run without the spike. Finally, in order to obtain basic data on breakup distance a faceplate and spike were run without a radome.

The basic data from each run was simply the amount of damage sustained by the model. The only other instrumentation available was photographic, and this was used to confirm model integrity during the experiment in case additional damage occurred as the sled was stopped after the test area. Figure 13 is a typical trackside photograph from run 5. It is interesting to note how clearly the region of separated flow is defined by the apparent pile-up of raindrops.

7.3 Results on the 4-Inch Radomes

7.3.1 Unprotected Radome at 3000 ft/sec.

Figure 14 and 15 show the unprotected 4-inch radome before and after the test. From Figure 15 it is apparent that the forward portion of the fiberglass radome was destroyed. A hole, approximately 2.5 inches in diameter was punched through the radome. A considerable portion of the remainder of the radome was eroded so that at no location is there any of the original outer surface remaining. The aluminum surface exterior to the radome was badly eroded, showing signs of being peened. It is interesting to note, although it is not shown in the photograph, that the center section of the aluminum plate is completely clear. From trackside streak photographs of this particular run and the accompanying radome erosion it is apparent that the destroyed dome was exposed to supersonic rain for a portion of the sled test. It must be concluded that the center section provided some degree of rain erosion protection through drop breakup. The rain erosion corresponding to 3000 feet per second is extremely severe for the fiberglass material used in these tests.

7.3.2 Spike-Protected Radome at 3000 ft/sec.

Figures 16 and 17 show the spike protected radome before and after a test essentially identical to that given the unprotected radome. While it is apparent that the structural integrity of the dome has been maintained, the dome did receive varying degrees of damage over its surface. There was relatively little damage in the center of the dome over an area included by a 1.5 inch circle. This clear region extended beyond the range of the tip cone and clearly resulted from the breakup action in the central portion of the dead air region. Damage increased beyond this point to a maximum at approximately the 45° point on the dome. Damage at this location varied from three to five layers of peeled fiberglass. Beyond the 45° station of the radome the damage decreased as the surface became aligned with the velocity of the vehicle. At the intersection of the radome with the base plate, a thin ring of material was cut out of the radome to a depth of approximately five layers.

The different degree of damage of various positions along the dome may be interpreted with the discussion of section 6.1 in mind. Near the center of the dome the distance over which the drop is acted on is comprised mainly of the distance between the separated layer and the dome. The distance between the edge of the mixing layer and the location of the end of drop breakup is approximately 4 inches. This distance diminishes to a minimum of 2 inches at the 75° location back along the dome. However, at this station the drops have little if any effect on the steeply inclined surface. The combination of varying effective breakup length and changing surface inclination leads to a location of maximum damage at approximately the 45° station. It is apparent that a dome which is harder than the fiberglass dome could be built to withstand the rain erosion damage in this size.

At the location where the fiberglass radome intersects the aluminum plate a thin ring of material was eroded. This is apparent in Figure 18. The most reasonable explanation of the erosion process is that the raindrops which strike the aluminum surface splatter out in all directions.

Those drops which impact adjacent to the radome flatten into a disc and the inner edge of this disc strikes the dome. This explanation is consistent with the fact that a thin ring of material was removed from the edge of the radome. It was not expected that this phenomenon would occur for spike geometries where the drop was completely broken up before impact.

Beyond the dome the drops are barely broken up by the conical shock wave and mixing layer and impact on the aluminum collar. As evidenced in Figure 17 the surface of the aluminum was badly pitted, demonstrating the destruction which the raindrops are capable of producing. This damage is in direct contrast to the protection afforded the dome by the separated region ahead of the fiberglass dome. This test was run twice with results which were identical for all practical purposes.

7.3.3 Spike-Protected Radome at Transonic Speeds

Below Mach number 1.27 the shock wave is no longer attached to the spike tip (assuming the present spike geometry). The flow behaves as if the spike were not there and forms a normal shock in front of the dome. Run 6 was conducted at transonic flow conditions to determine if the conditions of reduced velocity and normal shock were sufficient to protect the radome against rain erosion damage.

A post-test photograph of the transonic model is given in Figure 18. Note that except for a few scattered spots the radome is devoid of damage. It follows directly that rain erosion of this configuration is not a problem at transonic speeds.

There are several reasons why the drop damage is negligible at transonic speeds. First, the drop energy is smaller by an order of magnitude than the drop energy at the supersonic sled test conditions. Second, the drop breakup distance is weakly dependent on velocity such that a 4 inch breakup distance at Mach number 3 is approximately the same at low supersonic speeds.

Below Mach number 1.25 the bow shock is detached from the spike tip and is a blunt body shock. As the Mach number approaches unity this shock surface moves out away from the body providing a longer breakup distance. Below Mach number 1 the flow is subsonic potential flow. The stagnation line flow continuously compresses to the stagnation point. Drop breakup commences when the relative velocity between the drop and fluid corresponds to a Weber number above $(We)_{critical}$ for the raindrops.

7.4 Results on the 8-Inch Radome

Figure 19 shows the 8-inch spike-protected radome after a test at 3000 ft/sec. Note that the damage on the dome is asymmetric and the spike is bent. Trackside photographs of the spiked dome in flight reveal that the spike was straight while in the rain field and upon exit. It follows that damage to the dome from rain erosion should be symmetrical as it was in all previous runs.

At the end of the sled test run the sled is stopped by running the support slippers over a plastic sausage filled with water. The only logical explanation for asymmetrical damage and the bent spike is that the damage to the model occurred after exit from the rain field and probably during the water bag entry. Disregarding, then, the damage which apparently occurred while the sled was being stopped, the rain erosion damage on this radome is very slight. The minimum distance on this configuration between the mixing layer and the radome is 1 inches. Since this is about the breakup distance for 1.5 mm diameter drops predicted by equation 5.7, the lack of damage on this radome constitutes an excellent check on our quantitative model of spike protection.

7.5 Measurement of Breakup Distance with the Spike-Protected Faceplate

Figure 20 is a post-test photograph of the spike-protected faceplate. Since the decision to test it was made during the test program, this configuration was generated by sawing the 4-inch radome off an existing model. Four threaded holes and an annular slot fixed with fiberglass are shown in the photograph.

After the test, a series of measurements were made to determine the variation of surface roughness across the plate. The results are plotted in Figure 21 in terms of the standard deviation of surface pit depth. Surface roughness varies from less than 2 ten-thousandths at a radius of 7/8 inches to a maximum of 48 ten-thousandths at a radius of 2 3/8 inches. Beyond this radius surface roughness decreases to approximately 30 ten-thousandths, apparently because the drops peened the surface. At the rim of the plate, surface roughness is 43 ten-thousandths. No measurements were made of surface damage to the 0.25 inch thick fiberglass ring in the plate. The abscissa of Figure 21 is the breakup distance available between the dividing streamline in the mixing layer and the surface of the plate. It varies linearly from zero at the rim to 7" at the center, corresponding to the physical spike length.

The increase in surface roughness in going from the center to the rim of the plate is consistent with the discussion given above. Since both the critical drop diameter d* and the cut-off diameter d' are a function of the available drop breakup distance, they vary linearly from the rim to the center of the plate. Thus the (LWC) striking the plate increases from the center to the rim. If we assume, in the absence of better information, that the drop sizes in this artifical rain are distributed according to the (M-P) law described in Appendix B, the variation of (LWC) impact can be plotted directly as the universal curve of Figure B.1. The fit to the surface-roughness measurements is surprisingly good, since there is reason to expect that this roughness should be a linear function of the (LWC) impact.

The assumption that the drop size distribution in the sled test is similar to that of natural rain allows us at once to relate breakup distance to drop size. Where the (LWC) is reduced to half its total value, the cut-off drop size d' is by definition equal to the median volume diameter. If the 1.5 mm mean diameter quoted above for the Holloman track is indeed the median volume diameter, then for a separation distance X = 3 inches, we find that d' = 1.5 mm.

7.6 Comparison of the Sled-Test Result with the Correlation of Shock-Tube Measurements

Since the shock-tube experiments yield the drop diameter d* which is just broken up in the distance X_b and the sled tests yield the cut-off drop diameter d' which reduce the effective (LWC), a comparison of one with the other can yield a measure of the factor η which relates these two diameters.

The relevant test conditions for the spike-protected face plate were:

Mach number = 2.76
effective cone semivertex angle = 23°
altitude 4000 feet

The combination of Mach number and cone angle yield a ratio of density in the dead-air region to ambient density

$$\rho_a/\rho_\infty = 1.47 \qquad 7.1$$

The critical drop-size computed from equation 5.7 for X = 3 inches is then

$$d^* = 1 \text{ mm} \qquad 7.2$$

Comparing this with the value of d' obtained from the measurements of erosion on the face plate we obtain

$$\eta = \frac{d'}{d^*} = 1.5 \qquad 7.3$$

A value between 1 and 2 would be expected on the basis of the physical arguments presented above.

8. PREDICTIONS OF SPIKE-PROTECTED RADOME PERFORMANCE IN FLIGHT

Sled tests of spike-protected radomes are usefully only when their results can be extrapolated to predict performance in flight. This requirement, not the impossible wish to predict rain erosion from first principles, is the justification for the extensive analysis of test data reported above. Because the resistance of materials to damage by rain erosion cannot be predicted, a test will always be required before the performance of a new radome with spike protection can be evaluated.

Since the reduction in the effective (LWC) striking the radome depends on altitude but not on speed, the damage caused by rain erosion will be more severe with increased flight speed for both spike-protected and for unprotected radomes. Extrapolation of sled test data to flight altitudes can be done only at a fixed speed. Thus tests must be run at those speeds for which it is desired to establish operational limits for flight through rain.

The method of extrapolating sled test results to flight conditions will be described by applying it to the fiberglass radomes tests under this contract. The results will not represent a limit on the performance obtainable with spike protections. The fiberglass material used in these tests was not particularly resistant to rain erosion (as evidenced by the failure of the unprotected hemisphere, Figure 15). Improved performance of spike-protected radomes could be obtained simply by using a stronger radome material such as a ceramic.

8.1 The Permissible Amount of Water Striking the Radome

For the purpose of predicting flight performance, the end results of a sled test program for a given material at a given speed should be presented as the permissible amount of water striking the radome per unit area. This rate of water impact may be expressed in terms of the

effective (LWC) times the nautical miles flown. This computation yields the cumulative rain per unit surface area to which a radome is exposed.

An acceptable damage criterion is required before a quantitative limit of tolerable rain erosion damage can be established. For radomes this criterion would most logically be based on a measurement of the degradation of the radome performance. This kind of measurement was not available for the present tests. For the purpose of discussion we propose arbitrarily to state that the limit of acceptable damage was that encountered on the 8-inch radome. Since the rain erosion damage suffered by the 8-inch dome consisted of minor scattered spots over the surface of the dome, the requirement of low radar degradation and the actual damage are consistent.

The limit of acceptable damage established above must be correlated with the (LWC) striking the 8-inch radome. This is a function of the cut-off diameter d' defined in section 6.1. According to formula 6.4 the critical value of the separation distance between the radome and the mixing layer, based on a 20° semi-angle spike configuration, is 5.9 inches. At the track altitude of 4000 feet the critical drop diameter given by Figure 10 is

$$d^* = 2.0 \text{ mm} \qquad 8.1$$

and the cut-off diameter corresponding to the value of η observed in the tests of the spiked faceplate is

$$d' = 3.0 \text{ mm} \qquad 8.2$$

This is the largest drop size which the spiked radome can penetrate without exceeding the acceptable damage level.

As discussed in section 7.1 the natural rain rate corresponding to the median volume diameter encountered in the sled test is equivalent to 0.5 inches/hr. Based on this equivalence the (LWC) in the simulated rain is 10 times that encountered in natural rain. The effective water impact per unit area on the 8-inch radome may be obtained directly from the

chart of Figure 11. It is simply 10 times the value of the (LWC) for R = 0.5 in/hr and d' = 3 mm, or

$$I = 0.5 \text{ gram n. miles}/_{\text{meter}}^3 \qquad 8.3$$

8.2 Flight Performance Versus Rainfall Penetration and Altitude

Once the permissible water impact has been established, the allowable rain rates for radomes made of the same material may be computed for various altitudes and distances flown through the rain. For a given radome size, values of d' may be obtained from the curves of Figure 10 versus altitude. The required rainfall penetration determines the permissible (LWC) and hence, using the computed d', a value of the rain rate from Figure 11.

Performance curves for radome diameters of 8", 12" and 18" are presented in Figures 22-24. The allowable rain rates have been plotted versus altitude for a number of rainfall penetrations in nautical miles. Note that these should only be regarded as defining trends, since they are based on tests of a material which is not necessarily representative of the best erosion resistance material available.

In comparing the three figures, we see that better performance is obtained with the larger radomes. Figure 25 is a cross plot for 35,000 feet of the allowable rain rate versus radome size. The allowable rain rate on a bare radome is also shown. It is clear that at this altitude it makes no sense to design a spike-protected configuration unless the radome diameter is greater than 2.1 inches. This is almost always true in practice. Of course this value may be changed by using different radome materials.

For a given vehicle, Figures 22-24 show that the allowable rain rate drops off with altitude; the lighter air simply takes longer to break up the drops. Fortunately, the frequency with which heavy rain is encountered also drops off with altitude. Not much statistical data on the variation of rain rates is available and it is beyond the scope of this report to use it to derive design criteria.

As for the allowable rain rates at low altitudes, the value obtained indicate a very good probability of survival for missiles equipped with a spike protected radome. Figure 26 shows the fraction of the time during the year that missiles of several sizes can be flown various distances without encountering any degradation of the electrical performance of the radome. Again these curves represent trends rather than performance limits since they are based on the data obtained with the fiberglass used in the sled tests. Data on the frequency of various rain rates have been obtained from the Handbook of Geophysics (Reference 14) and represents average conditions in the continental U. S. A. A tremendous variation exists from one geophysical location to another and hence the effectiveness of the spike must be evaluated in terms of the rain statistics of the location where the spike might be used.

9. REFERENCES

1. Figler, B. D., Parkin, W. J., Wilson, J. C., Rain Erosion Suppression at Supersonic Speeds. (U), MITHRAS Report MC-61-6-R1, Cambridge, Mass., October, 1962.

2. Figler, B. D. A Solution to the Problem of Rain Erosion at Supersonic Speeds (U), MITHRAS Report MC-61-6-R2. Cambridge, Mass., October, 1963.

3. Fyall, A. A. and Strain, R. N. C. A "Whirling Arm" Test Rig for the Assessment of the Rain Erosion of Materials, Royal Aircraft Establishment Report No. Chem. 509, Dec. 1956.

4. Dunn, C. E. Results of Testing Slip Cast Fused Silica Radomes Under Rain Environment General Dynamics Division Technical Memorandum TM No. 6-223-571, July 1963.

5. Lane, W. R., Shatter of Drops in Streams of Air, Industrial and Engineering Chemistry, Vol. 43, No. 6, pp 1312-1317, 1951 (U).

6. Rupe, J. H., A Technique for the Investigation of Spray Characteristics of Constant Flow Nozzles, Part I. Paper presented at Conference on Fuel Sprays, University of Michigan, March 1949 (U).

7. Hanson, A. R., Domich, E. G. and Adams, H. S. An Experimental Investigation of Impact and Shock-Wave Breakup of Liquid Drops. Final Report T8881, University of Minnesota, November, 1955 (U).

8. Hanson, A. R., Domich, E. G. and Adams, H. S., Accoustical Liquid Drop Holder, Review of Scientific Instruments, Vol. 35, No. 8, August 1964. (U).

9. Clark, B. J., Breakup of a Liquid Jet in a Transfer of Gas, NASA TN D-2424, August 1964.

10. Engel, O. G., Fragmentation of Waterdrops in the Zone Behind an Air Shock, Journal of Res. of the Nat. Bur. of Standards, Vol. 60, No. 3, March 1958, Research Paper 2842 (U).

11. Gordon, G. D., Mechanism and Speed of Breakup of Drops, Journal of Applied Physics, Vol. 30, No. 11 November 1959 (U).

REFERENCES (Continued)

12. Ruetenik, J. Ray and Witmer, Emmett, A., Transient Aerodynamics of Two-Dimensional Air Foils. Part I MIT Aircraft Lab. August 1956. WADC Tech Report 54-368, Part I.

13. Holloman Track Capabilities, Technical Documentary Report No. MDC-TDR-62-9, September 1962 (U).

14. Handbook of Geophysics. Revised Edition MacMillan Company 1960.

TABLE 1

SUMMARY OF SHOCK TUBE TEST CONDITIONS

DRIVER PRESSURE (PSIA)	DRIVEN PRESSURE (PSIA)	DRIVER GAS	V_s (FPS)	q_2 (PSIA)	M_2	DROP SIZE (INCHES)
30	1.50	AIR	2040	2.67	.839	.060-.070
60	2.90	AIR	2050	5.35	.839	.068-.078
120	6.0	AIR	2040	10.7	.839	.071
141	2.98	AIR	2400	10.5	1.06	.070*
38	1.0	He	3130	10.5	1.32	.070*
103	2.8	He	3080	28.4	1.32	.070*

* ASSUMED - LARGE FIELD OF VIEW

TABLE 2

SLED TEST RUN SCHEDULE

RUN	CONFIGURATION	DOME DIAMETER, D_c (INCHES)	L/D_c	ENTRY V(CPS) M	EXIT V(CPS) M	COMMENTS
1	Spiked-Dome-Collar	4	7/6	3040 2.77	2970 2.70	Max Damage AT45° Slayers Eroded
2	Spiked-Dome-Collar	4	7/6	3030 2.73	2950 2.60	Repeat of 1
3	Unspiked-Dome-Collar	0	0	2930 2.62	2830 2.53	Dome Destroyed
4	Spiked Flat Plate	0	7/6	3040 2.76	3030 2.73	4" Breakup Distance
5	Spiked-Dome-Collar	8	7/6	1450	765	Spike Bent After Exit. Dome Damage During Breakup Clear Area 30°
6	Spiked-Dome-Collar	4	7/6	2970 AVG		About 10 Scattered Spots

CONFIDENTIAL

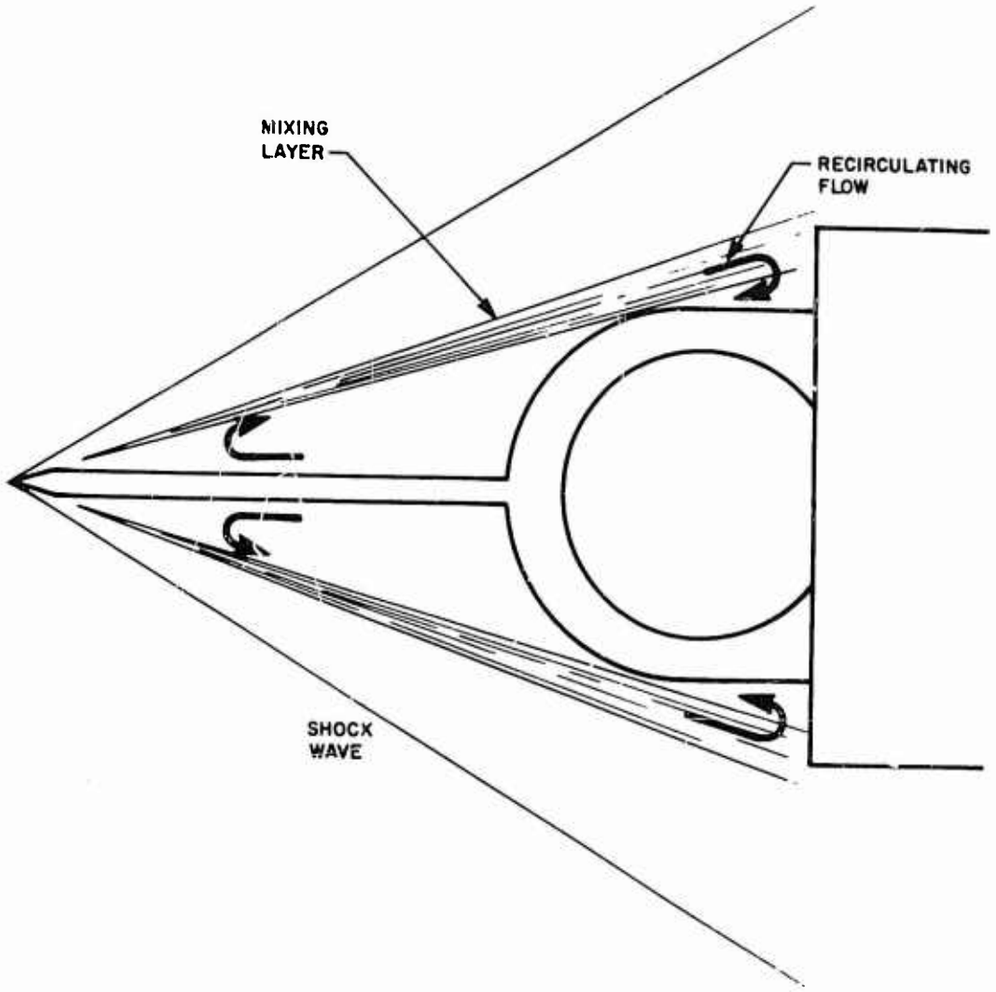

Figure 1. Spiked Induced Flow Pattern.

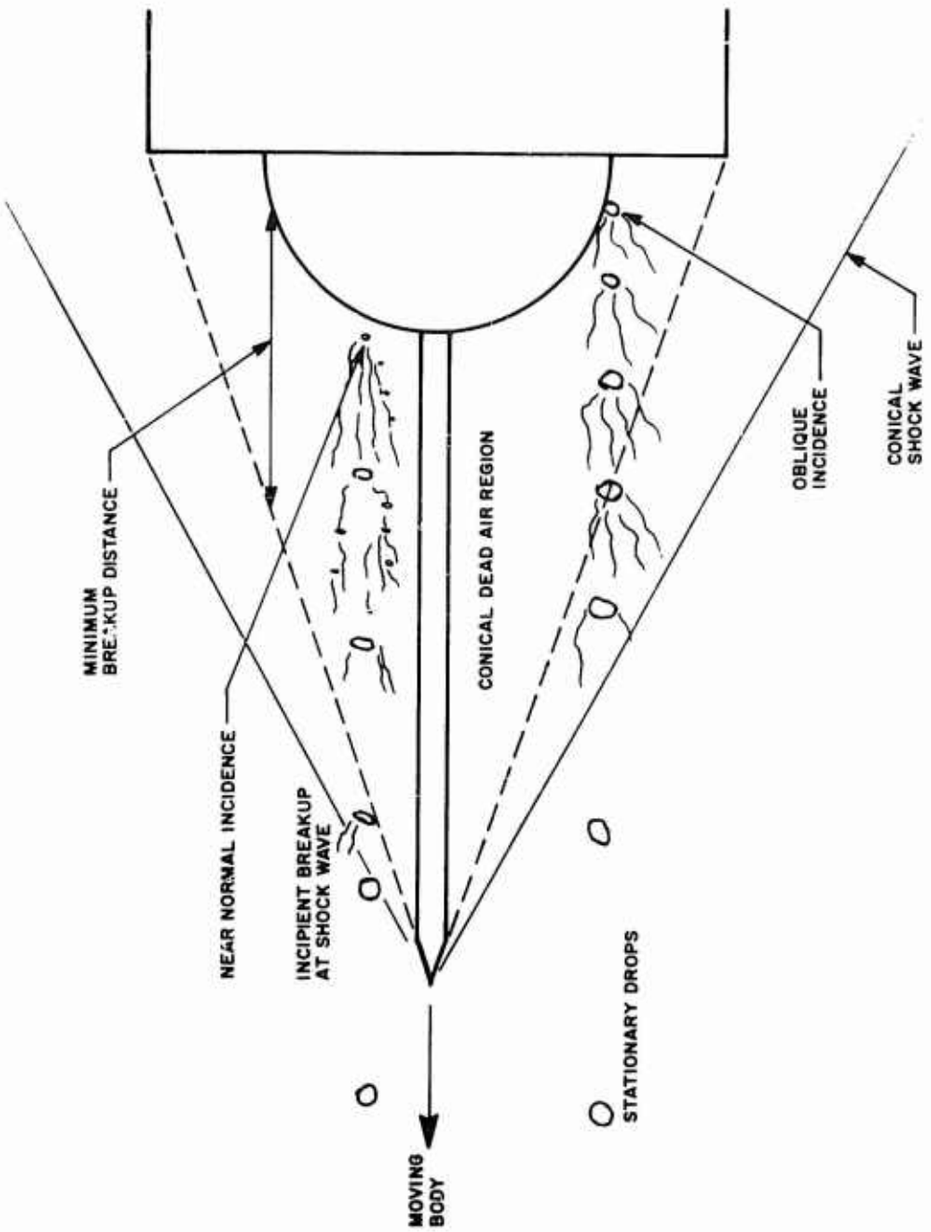

Figure 2. Schematic of Drop Breakup by a Spike Induced Separated Flow.

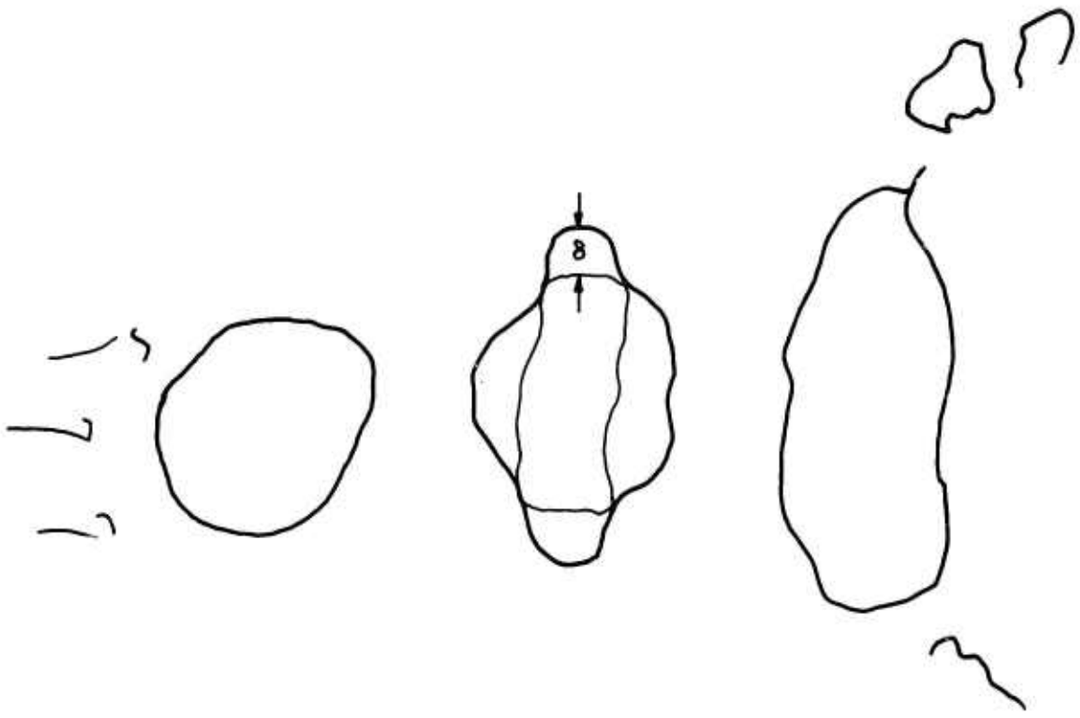

Figure 3. Drop Distortion Model.

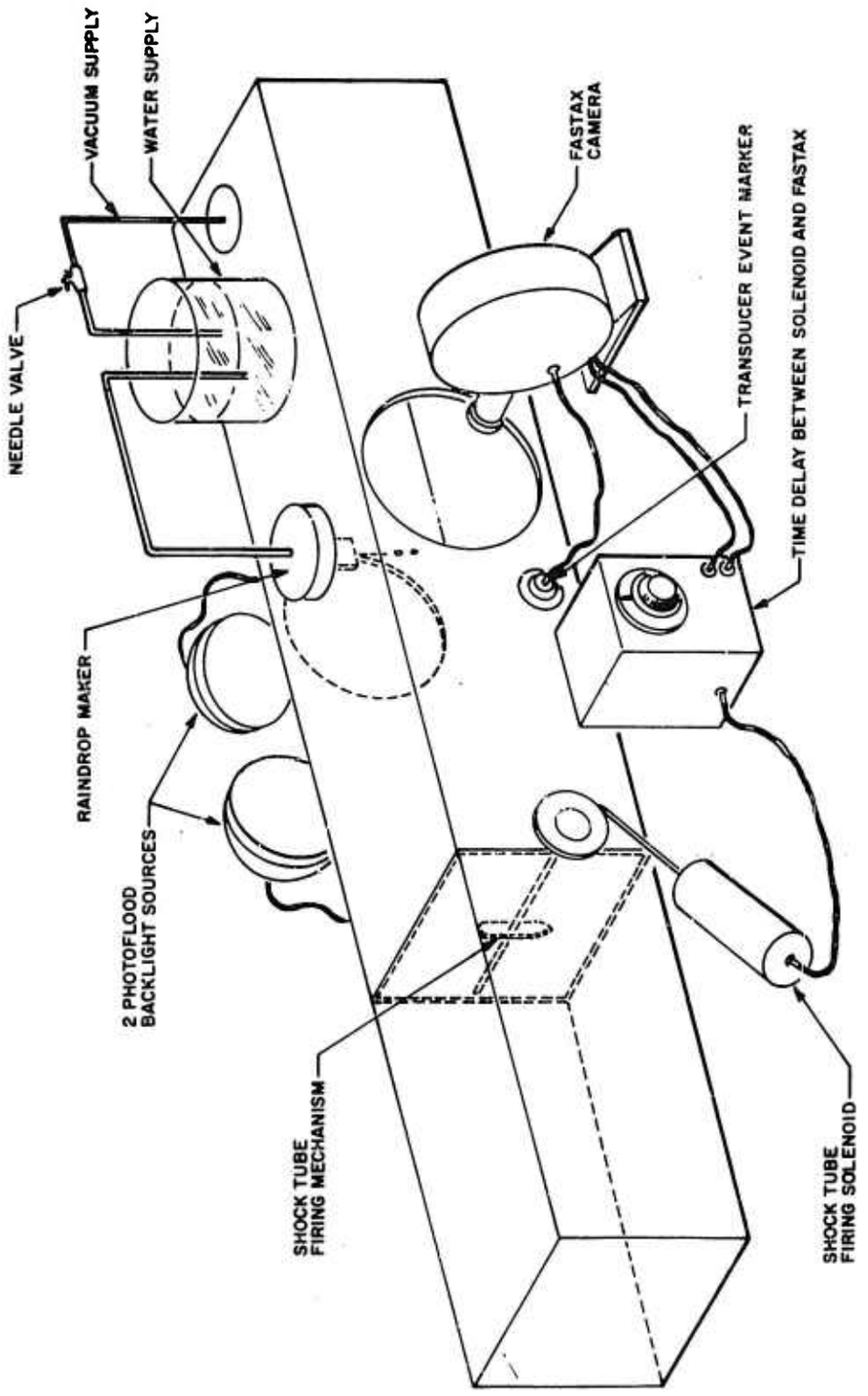

Figure 4. Schematic of Shock Tube Experiment.

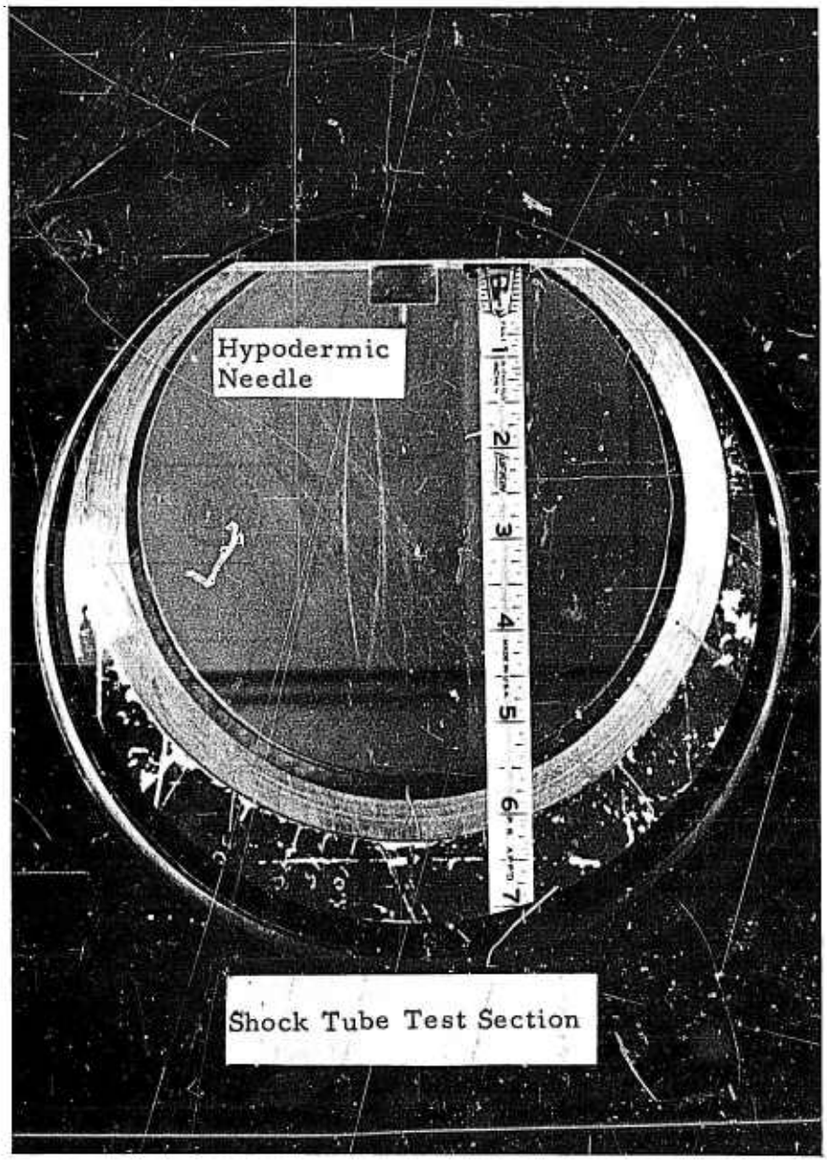

Figure 5a. Dropmaker Apparatus.

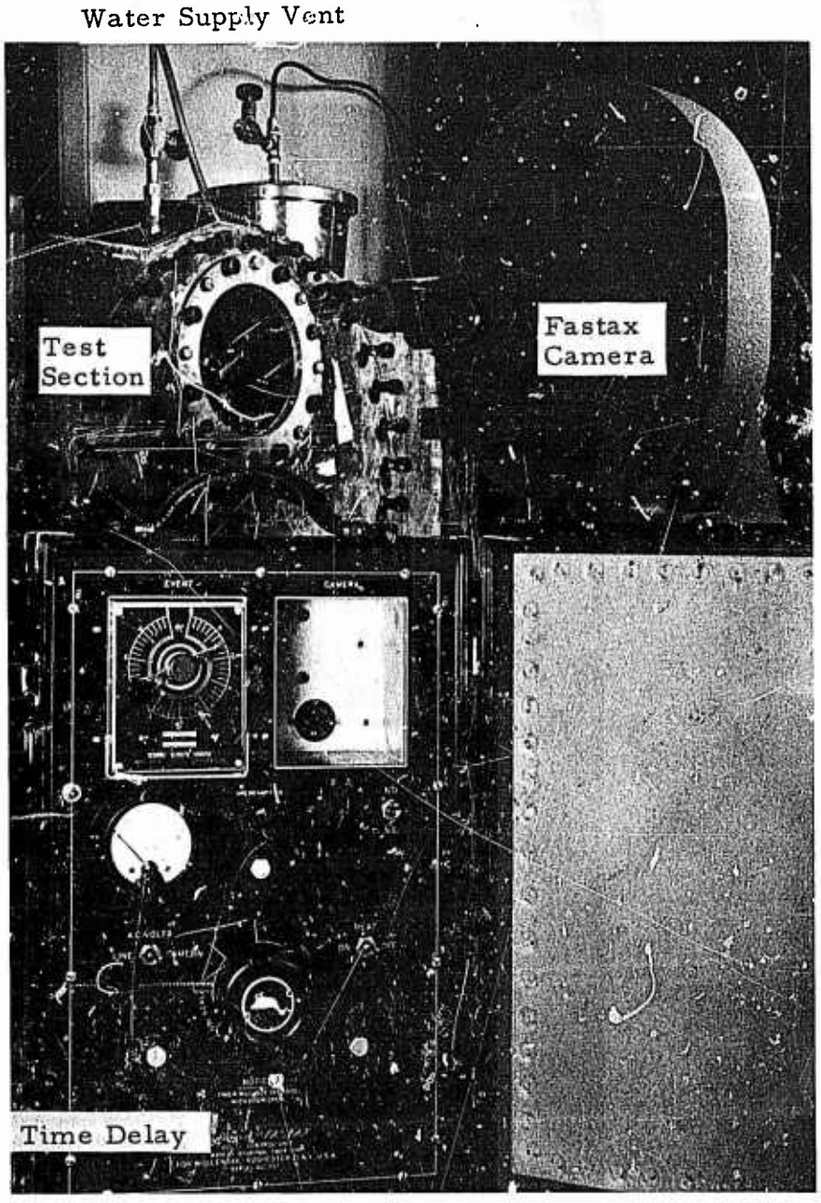

Figure 5b. Test Equipment.

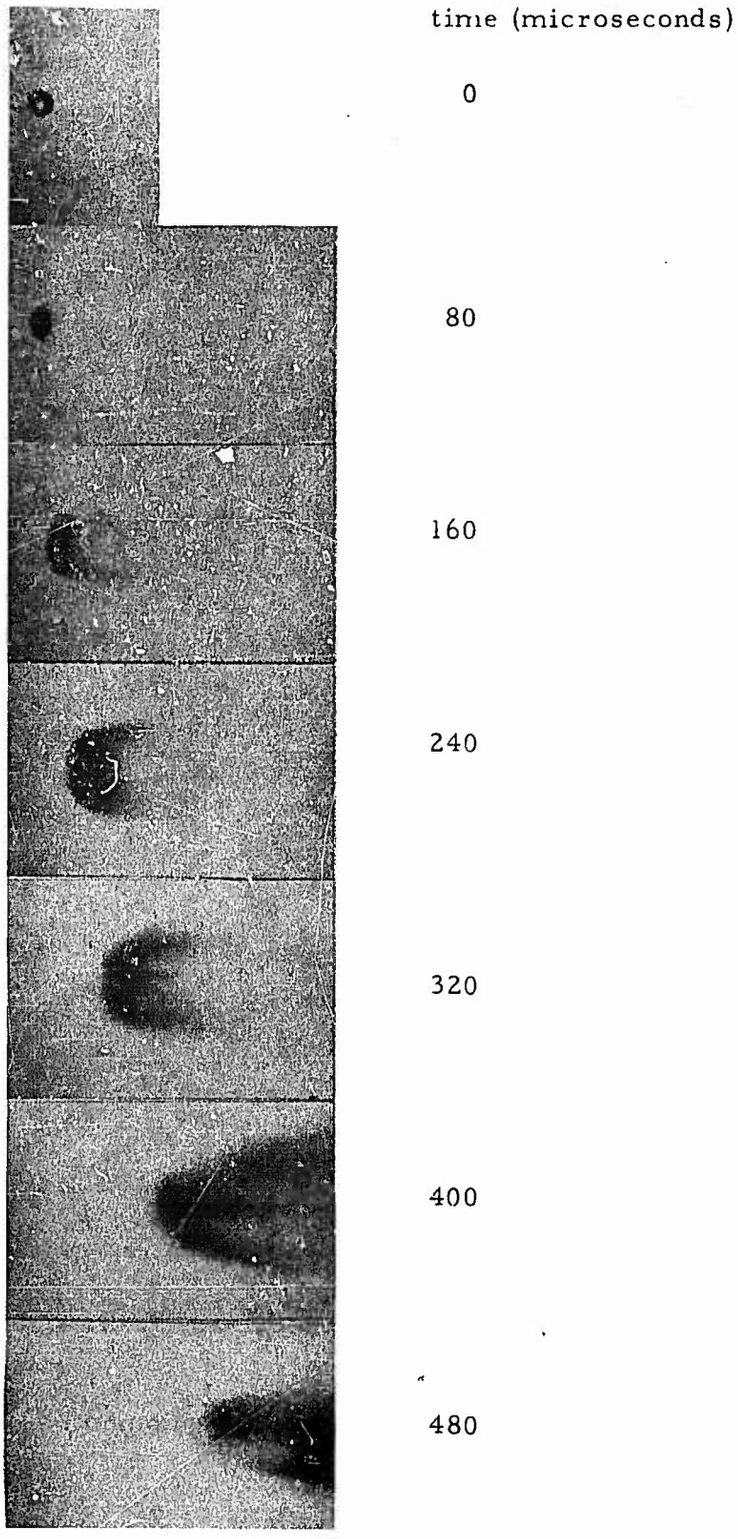

Figure 6. Sequential Photographs of Drop Breakup.

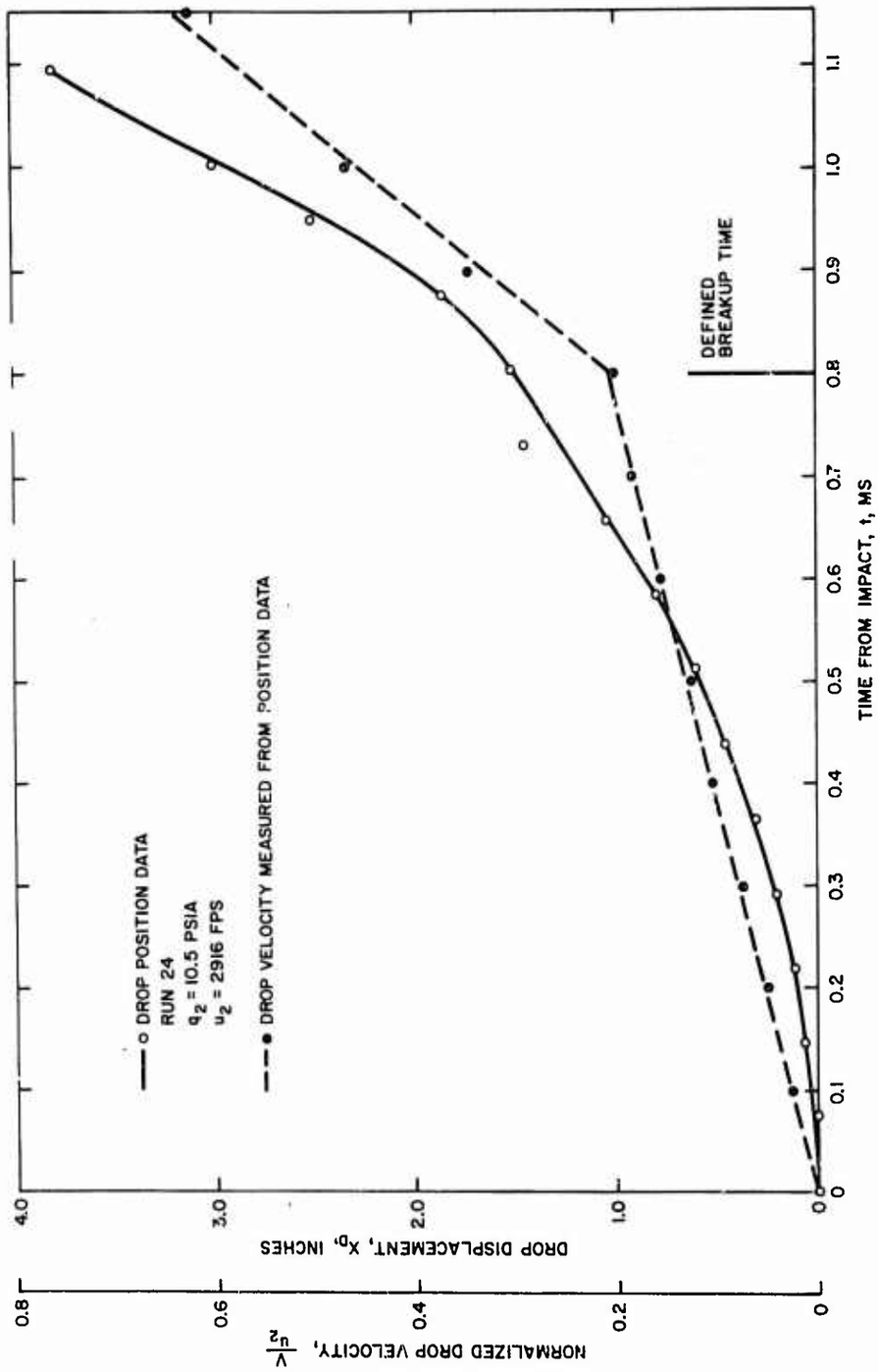

Figure 7. Drop Displacement and Velocity Versus Time.

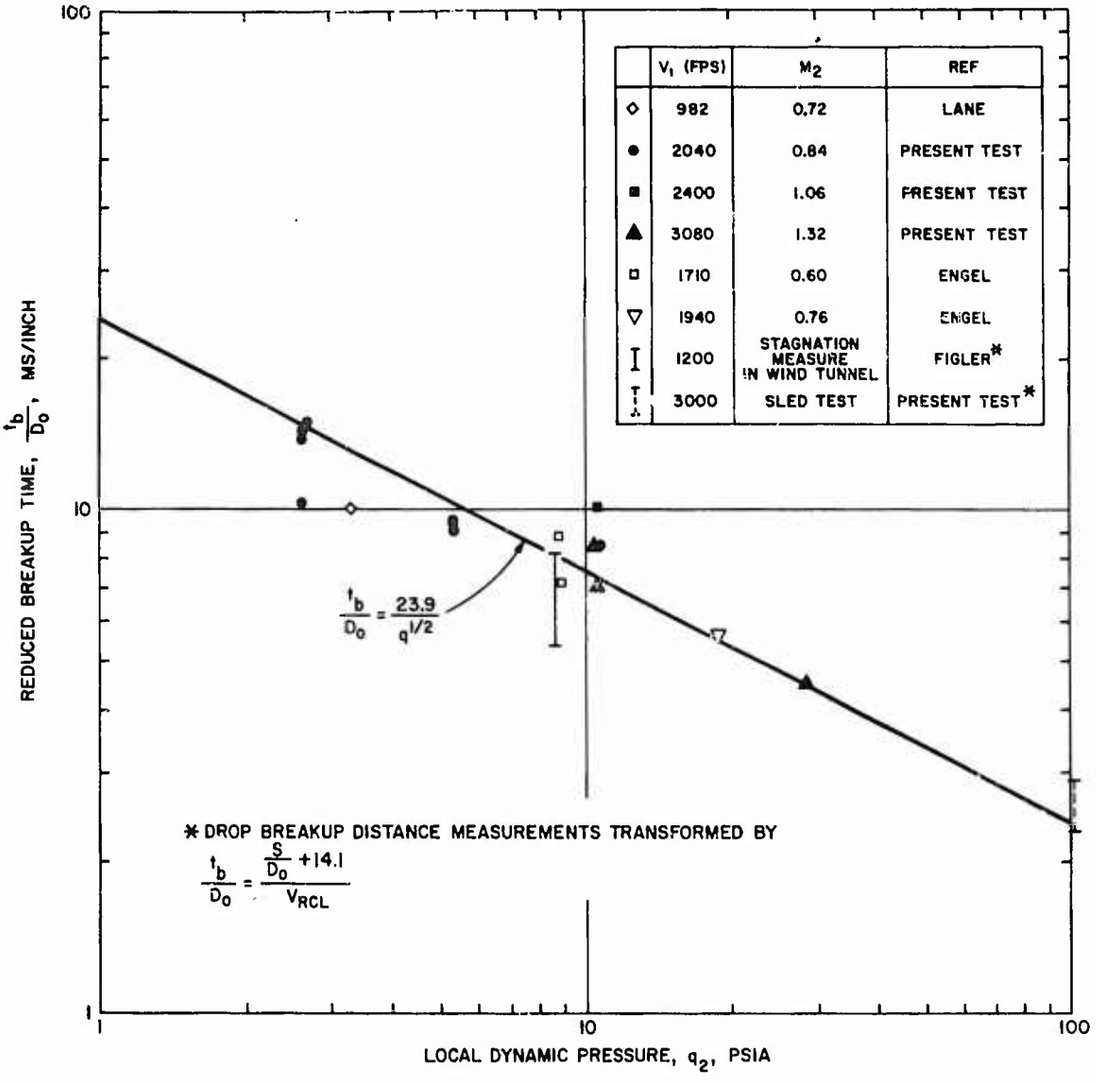

Figure 8. Summary Plot of Drop Breakup Time Versus Dynamic Pressure.

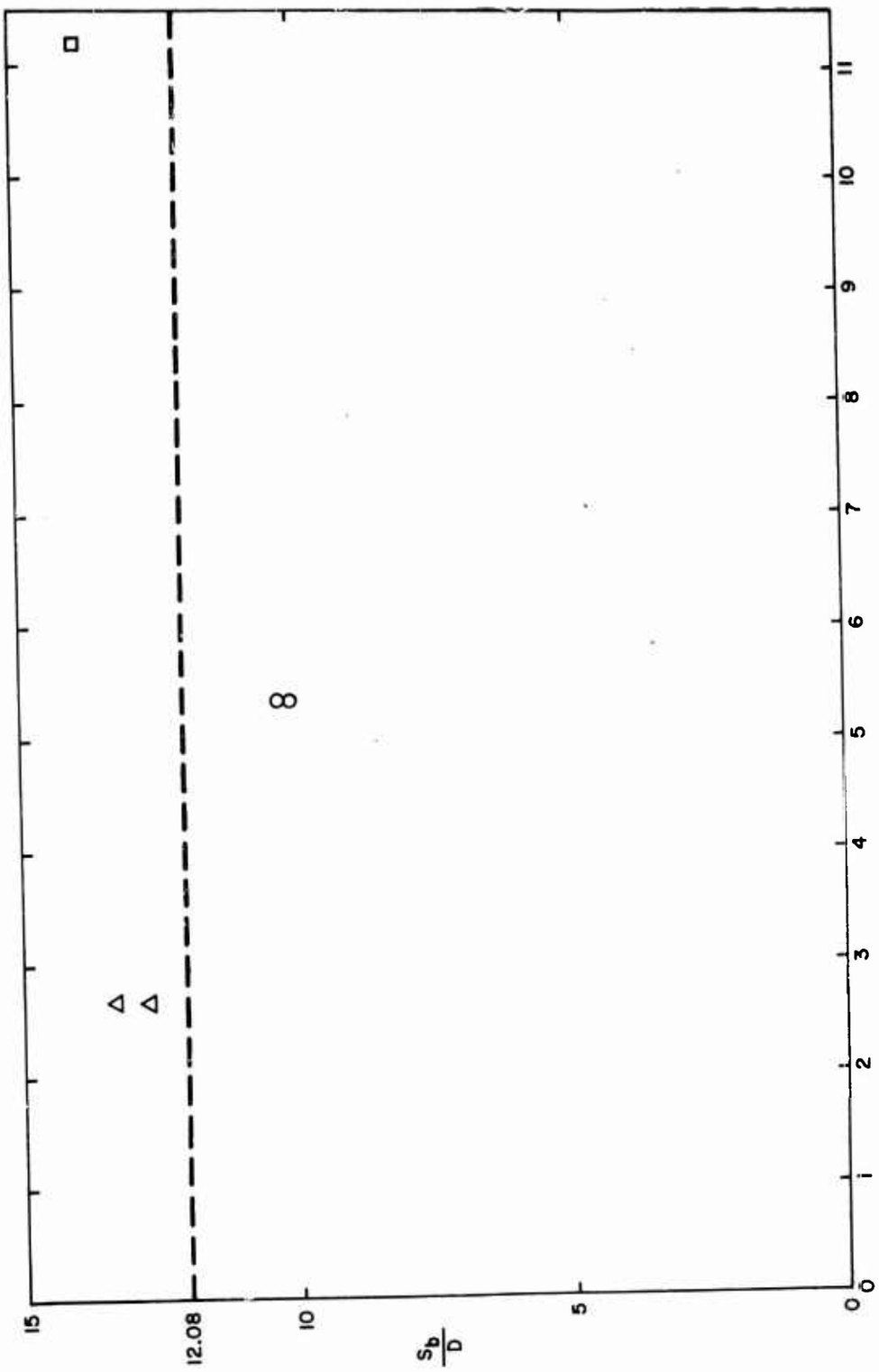

Figure 9. Drop Displacement Versus Dynamic Pressure.

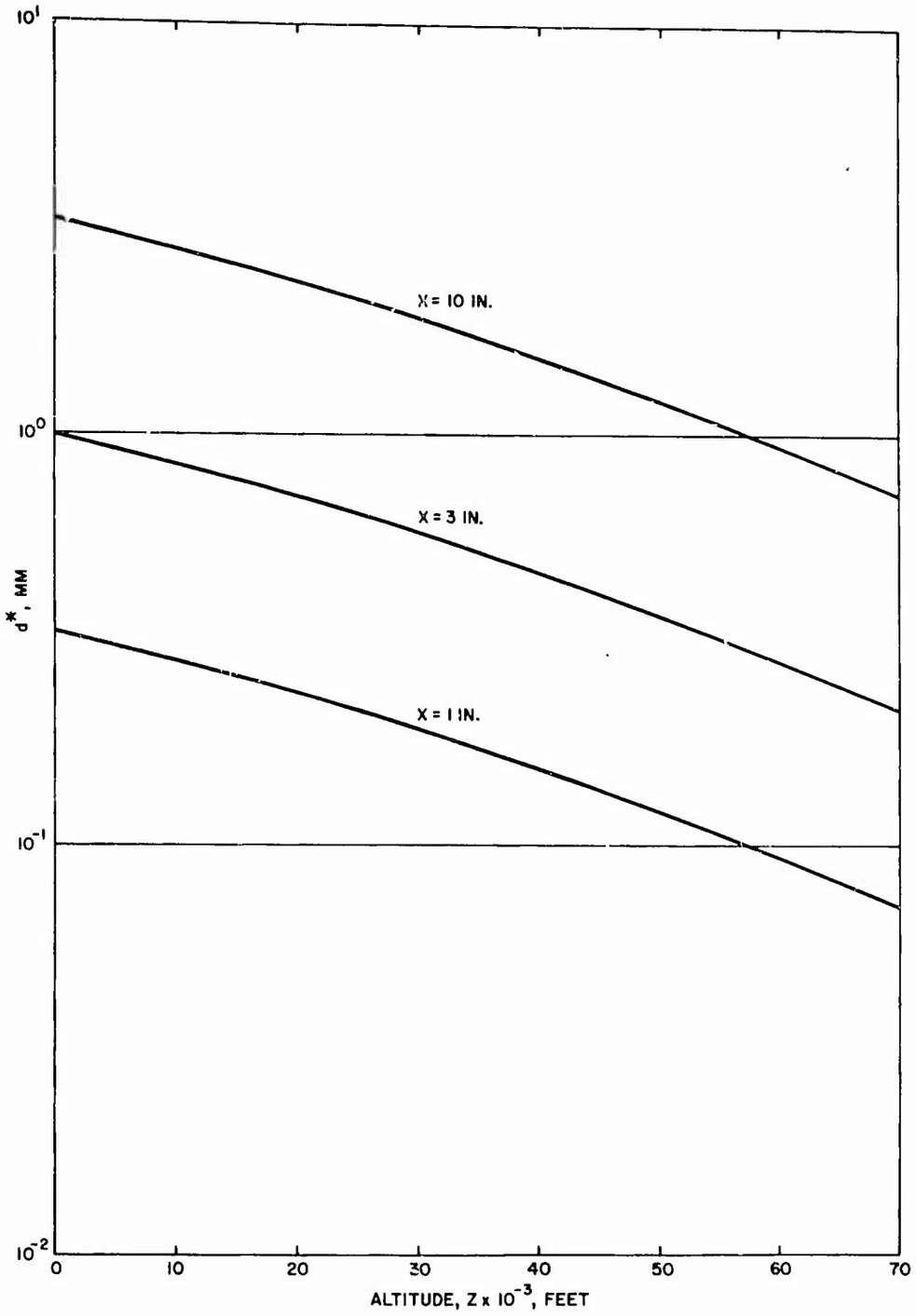

Figure 10. Critical Drop Diameter d^* Versus Altitude.

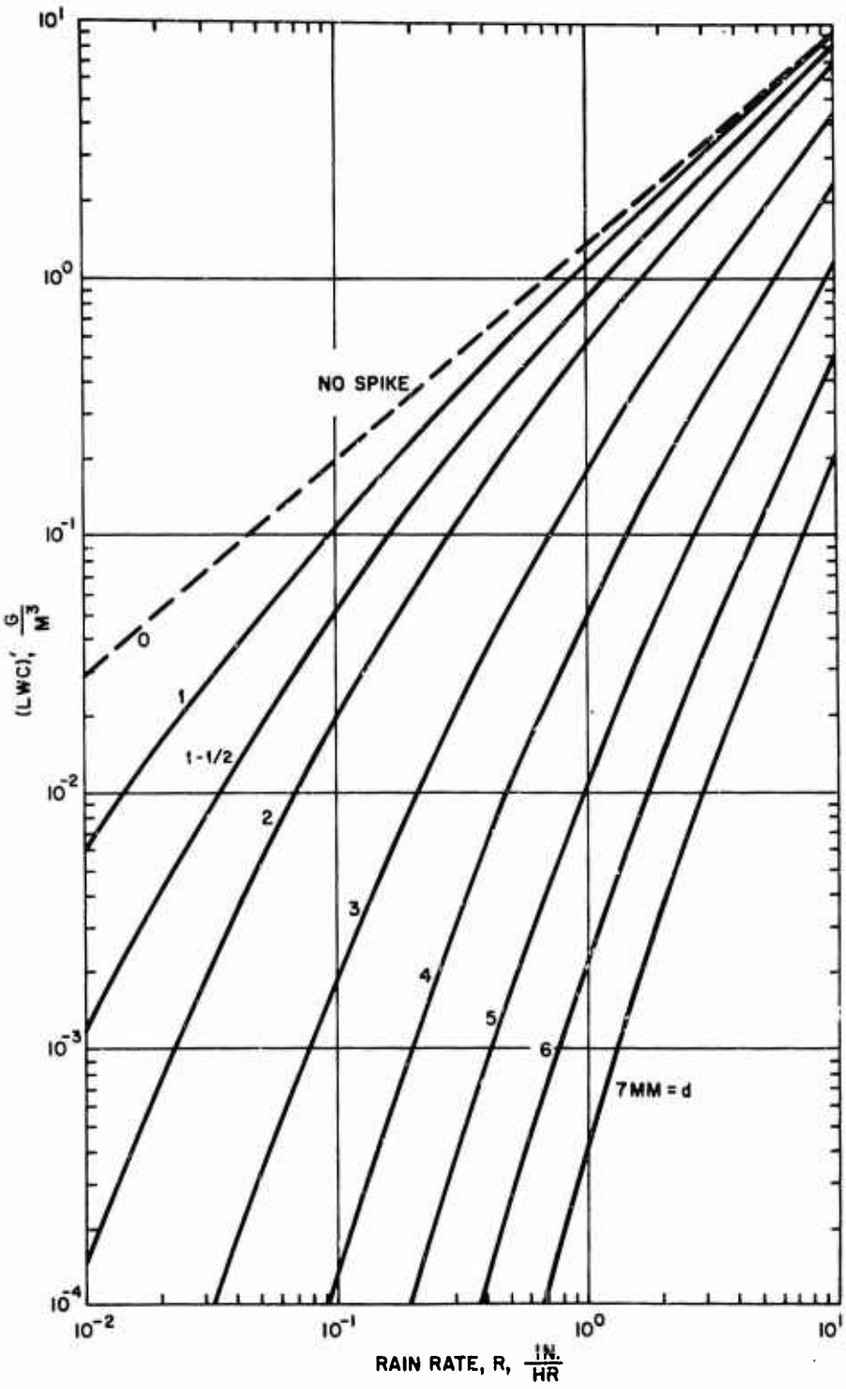

Figure 11. Effective (LWC) Versus Rain Rate for Several Values of Cut-Off Diameter.

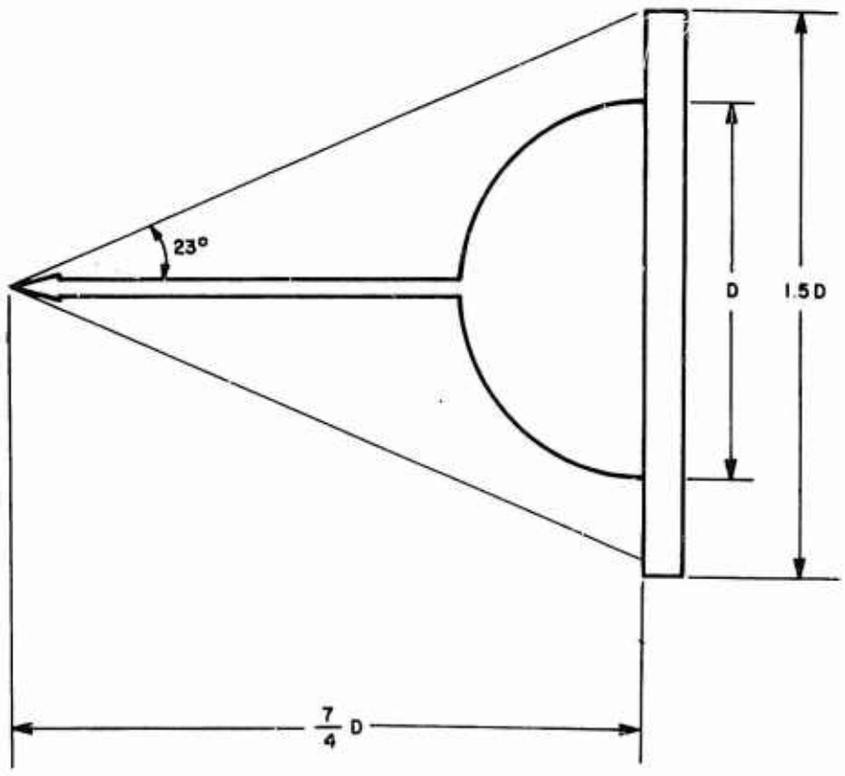

Figure 12. Drawing of Sled Test Radome Geometry.

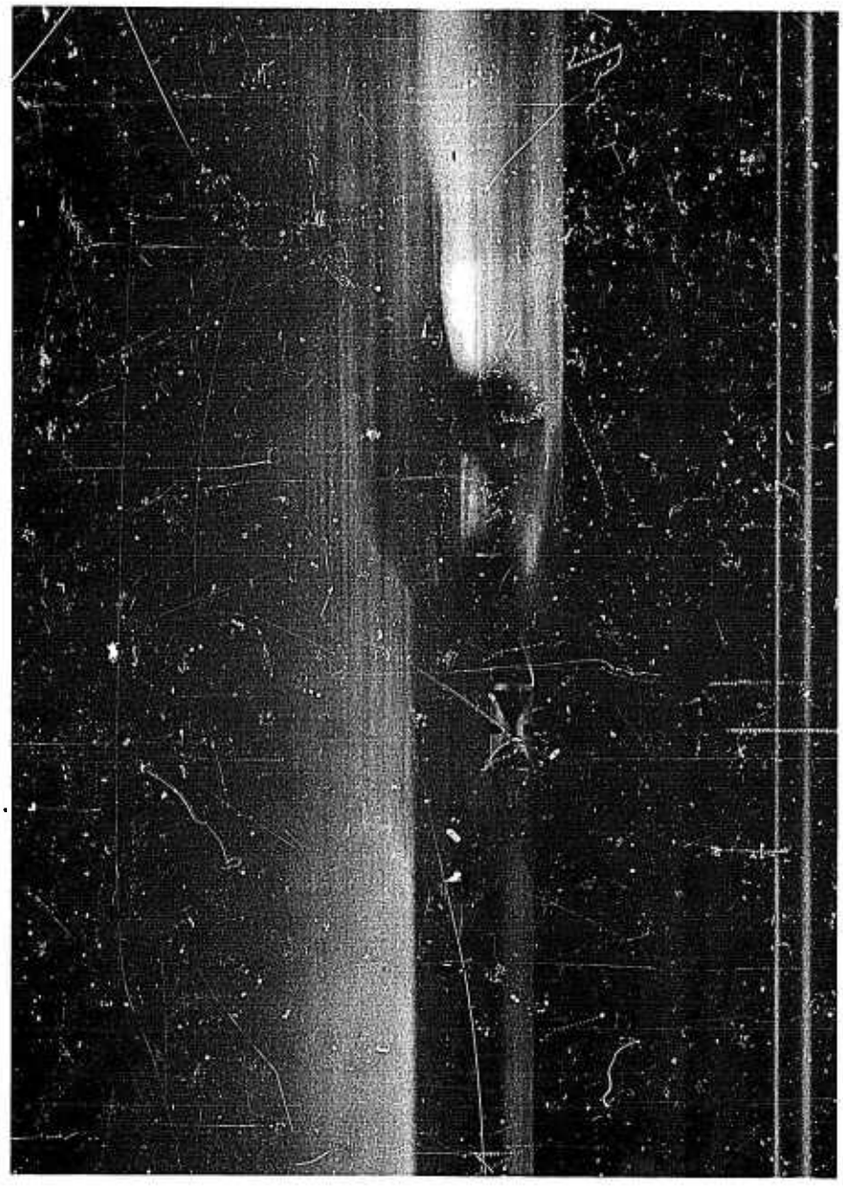

Figure 13. Trackside photograph of supersonic SDC configuration in the rain field.

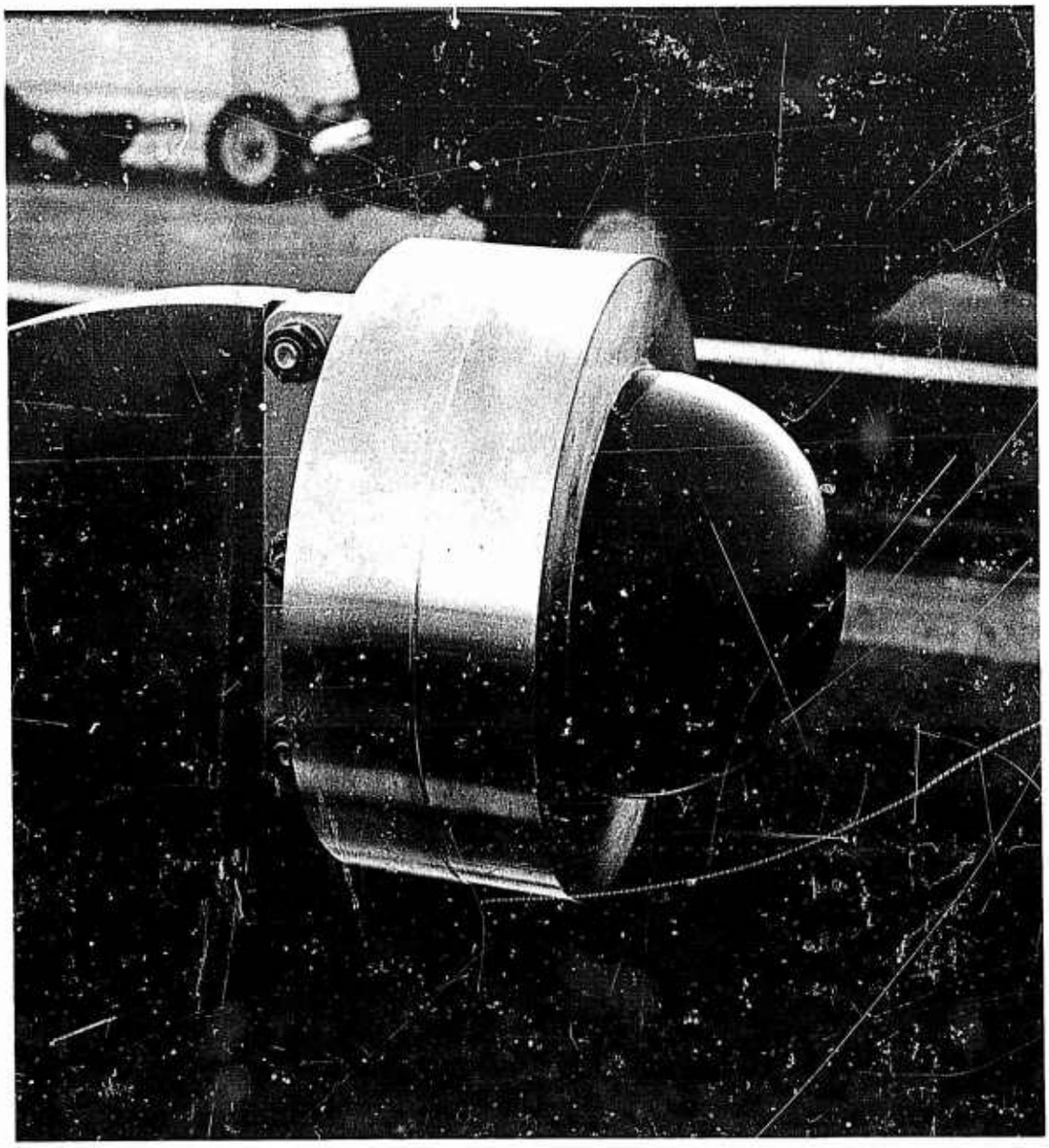

Figure 14. Unspiked dome collar configuration - before firing, run 3.

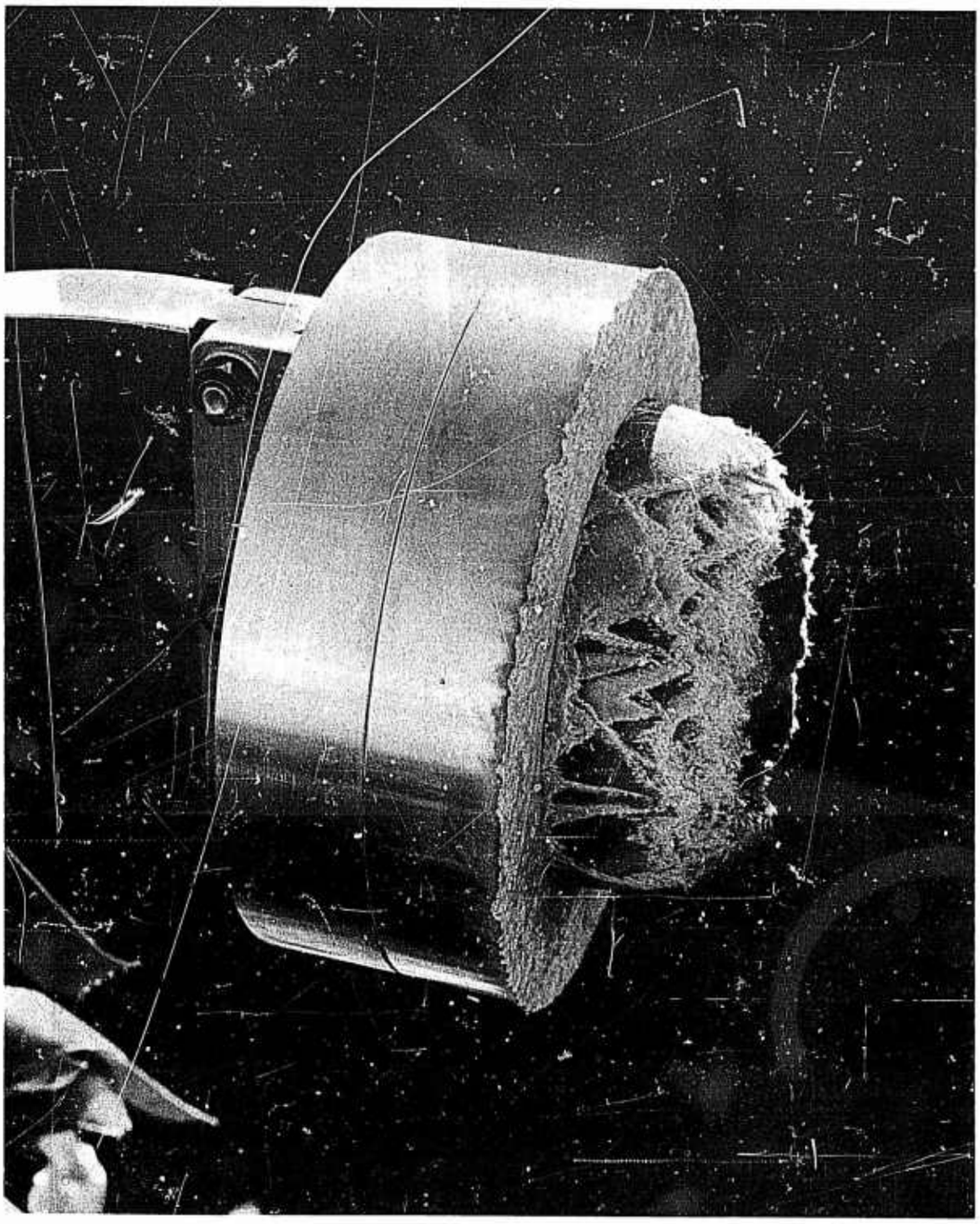

Figure 15. Unspiked dome collar configuration - after firing, run 3.

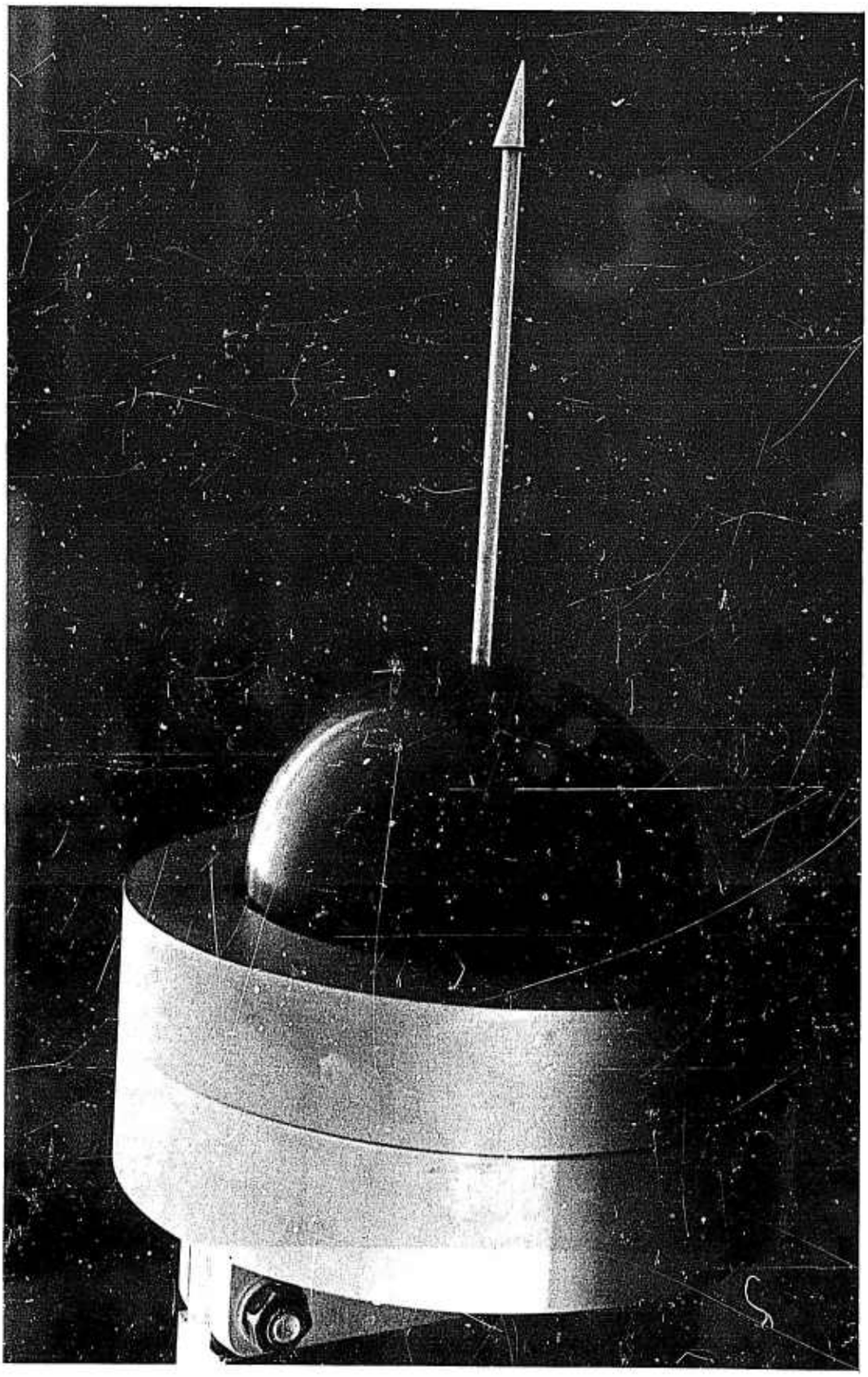

Figure 16. S-D-C Configuration with 4 inch radome - before firing, run 1.

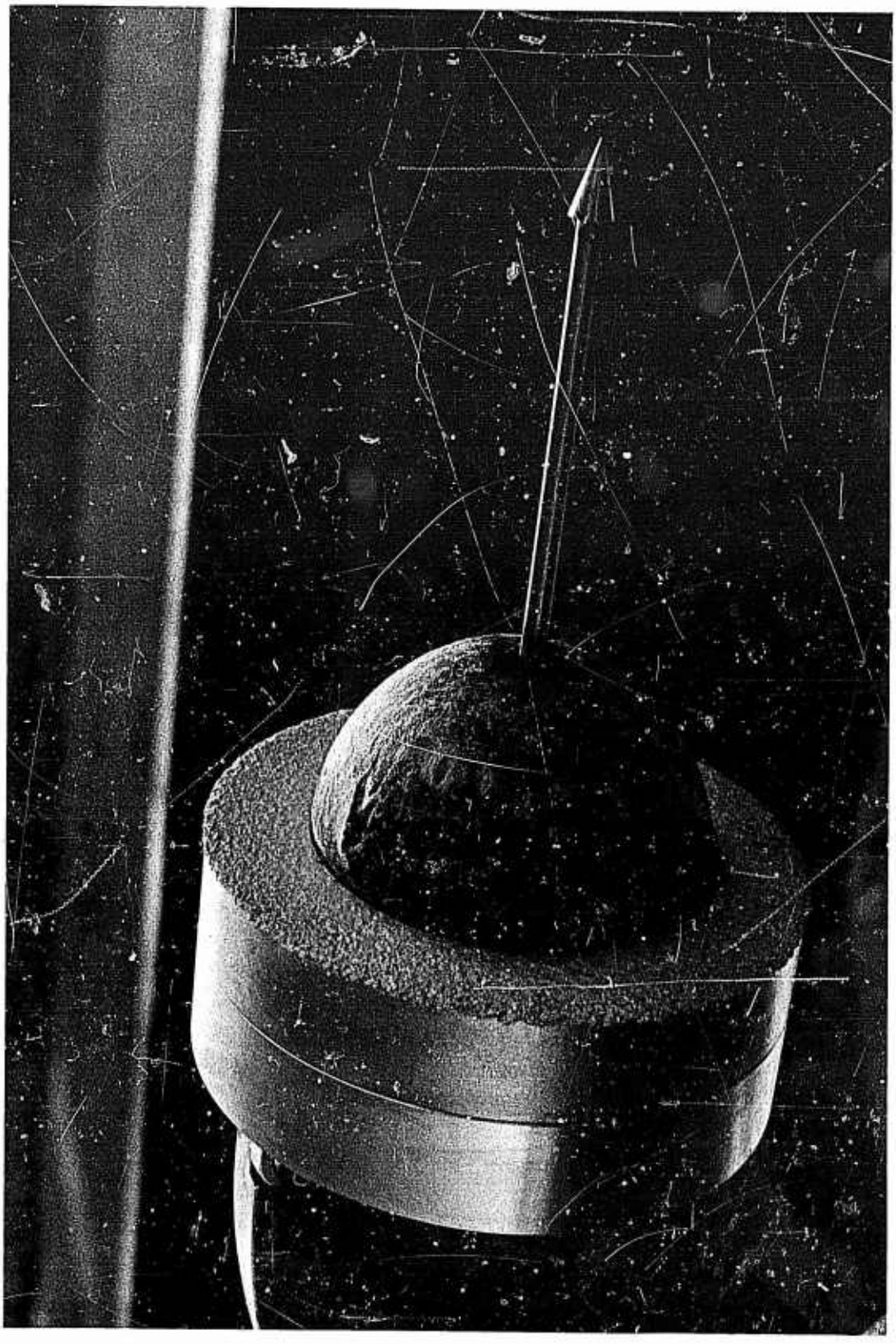

Figure 17. S-D-C Configuration with 4 inch radome-after firing, run 1.

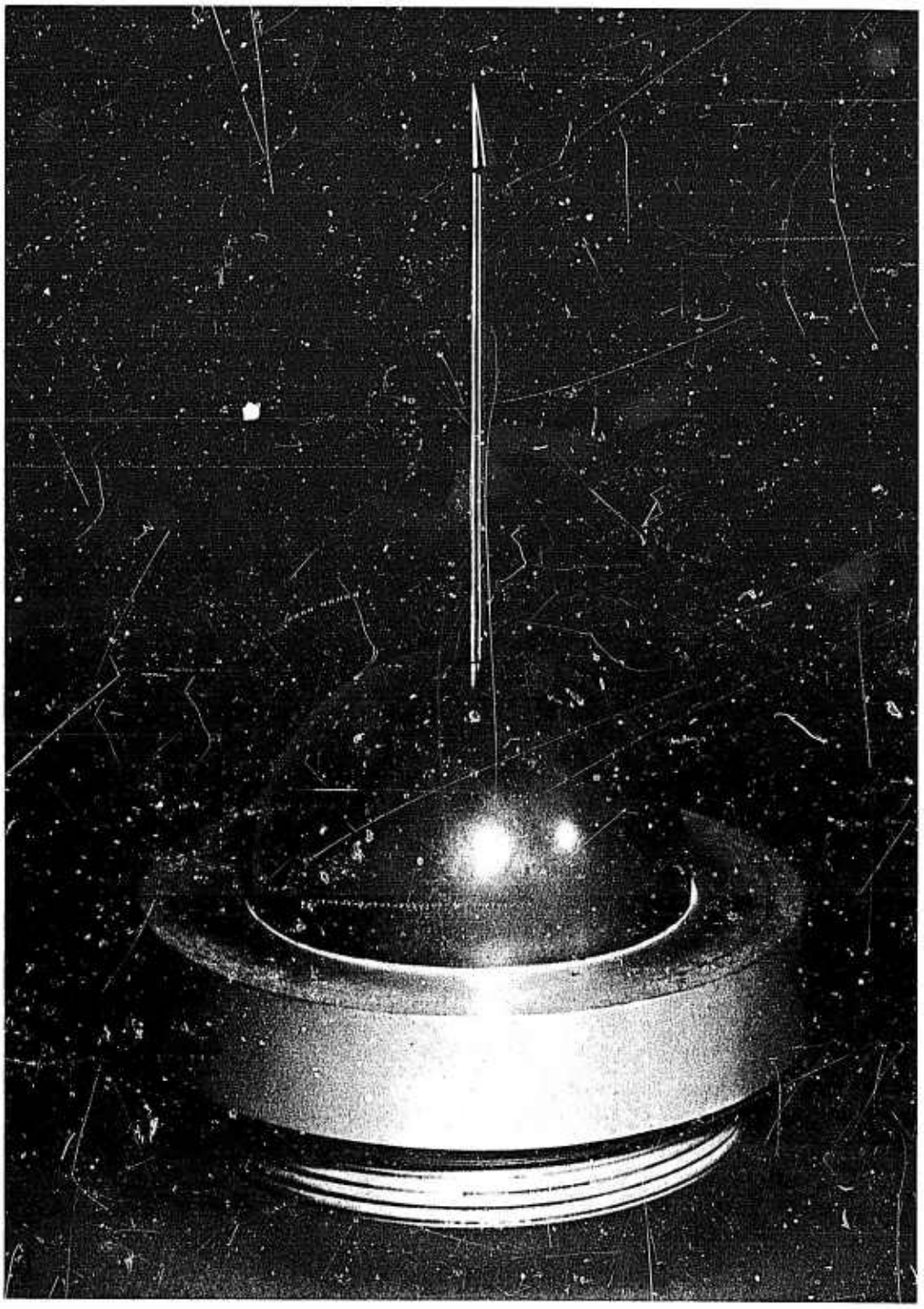

Figure 18. Post-Test Photograph of 4-Inch Transonic Model.

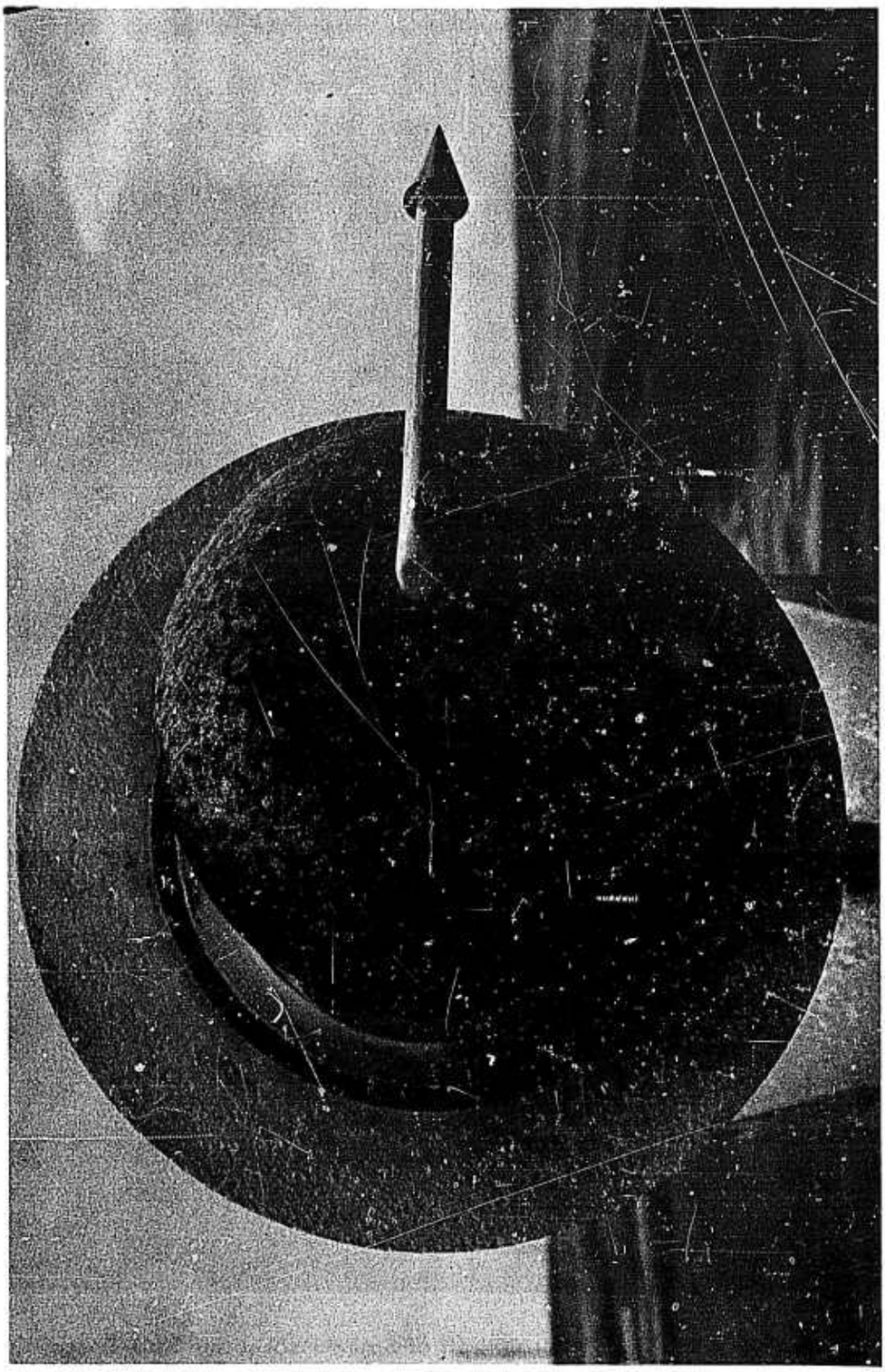

Figure 19. Eight-inch spiked hemisphere sled test.

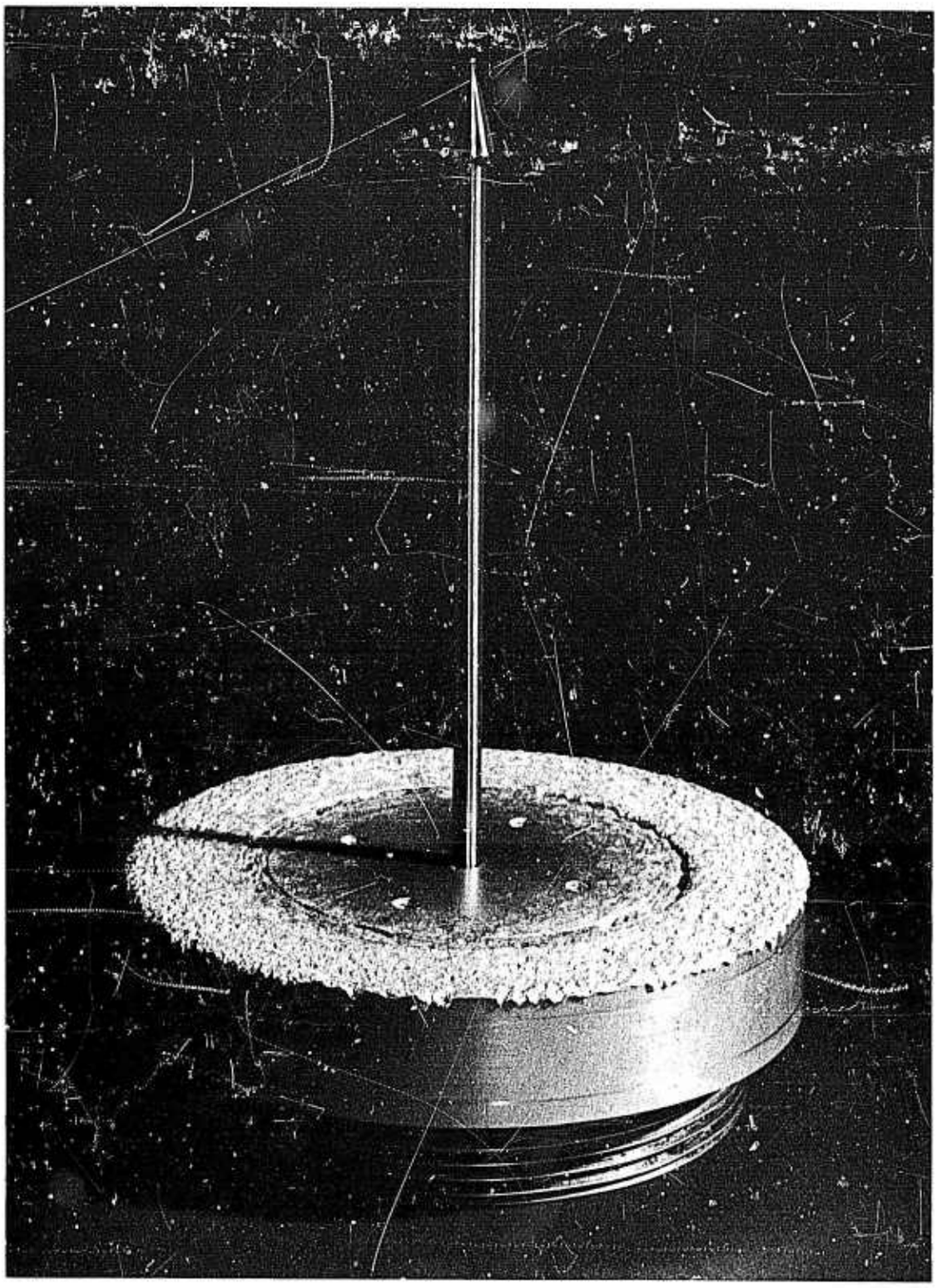

Figure 20. Post-Test Photograph of Spike Protected Flat Plate.

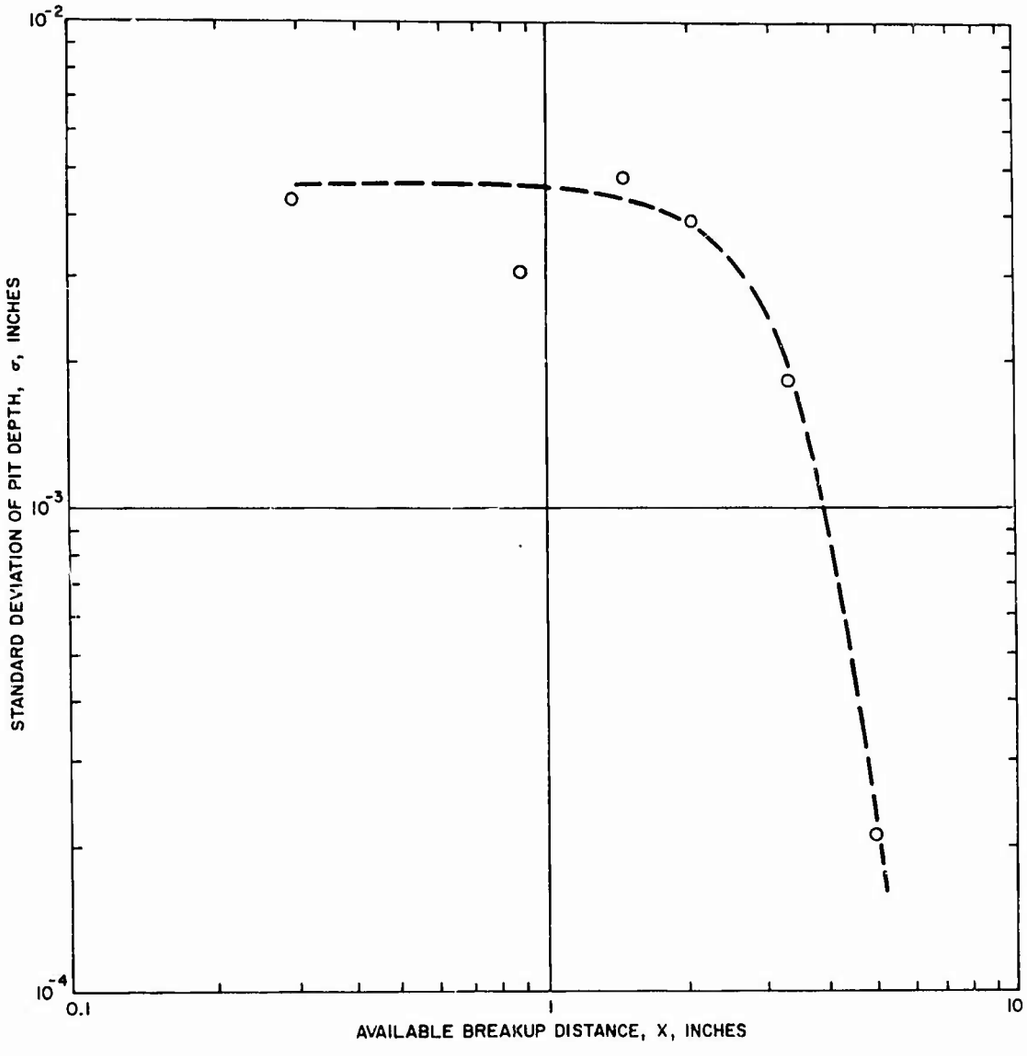

Figure 21. Flat Plate Surface Roughness Distribution.

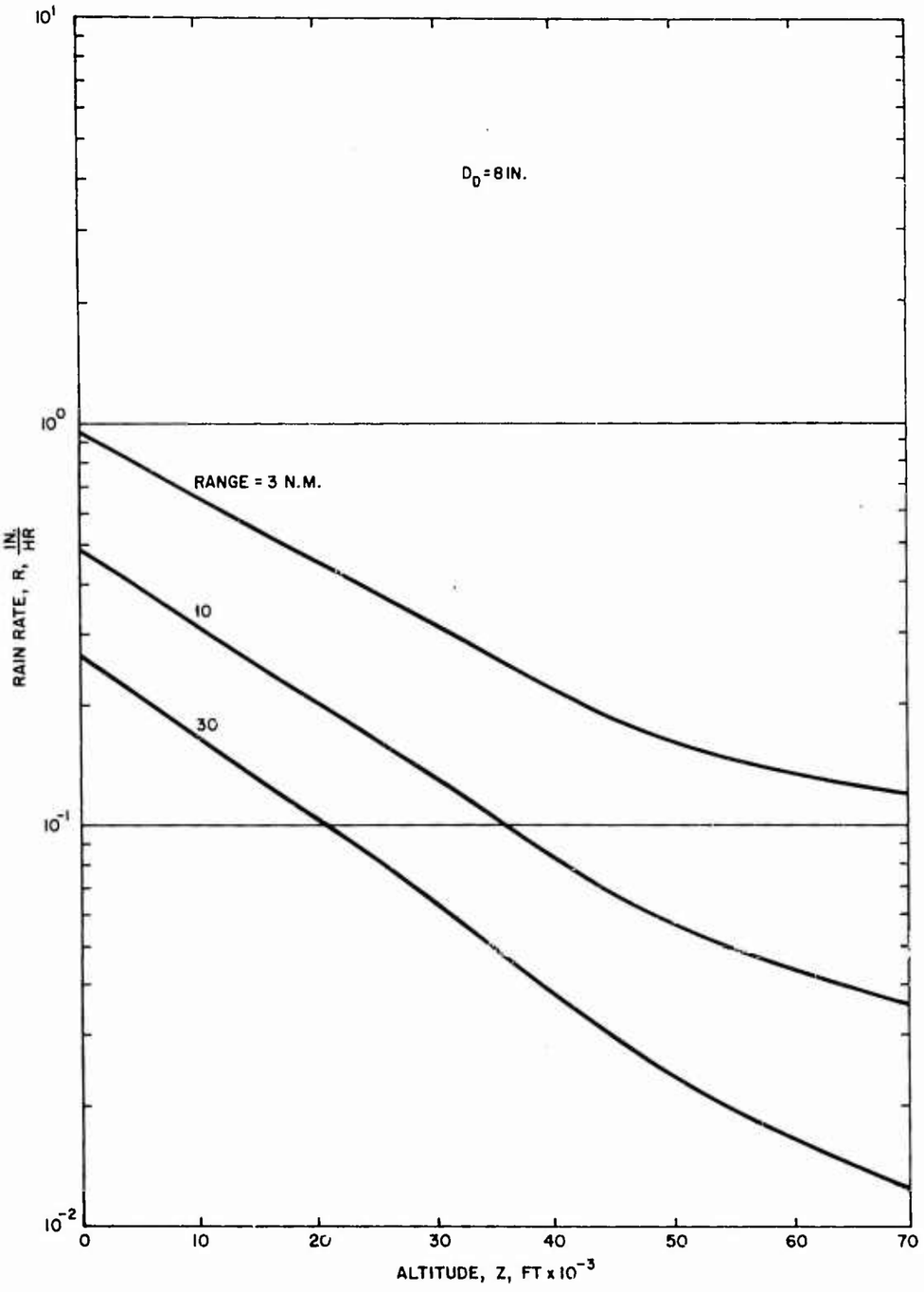

Figure 22. Allowable Rain Rate Versus Altitude for an 8-Inch Radome.

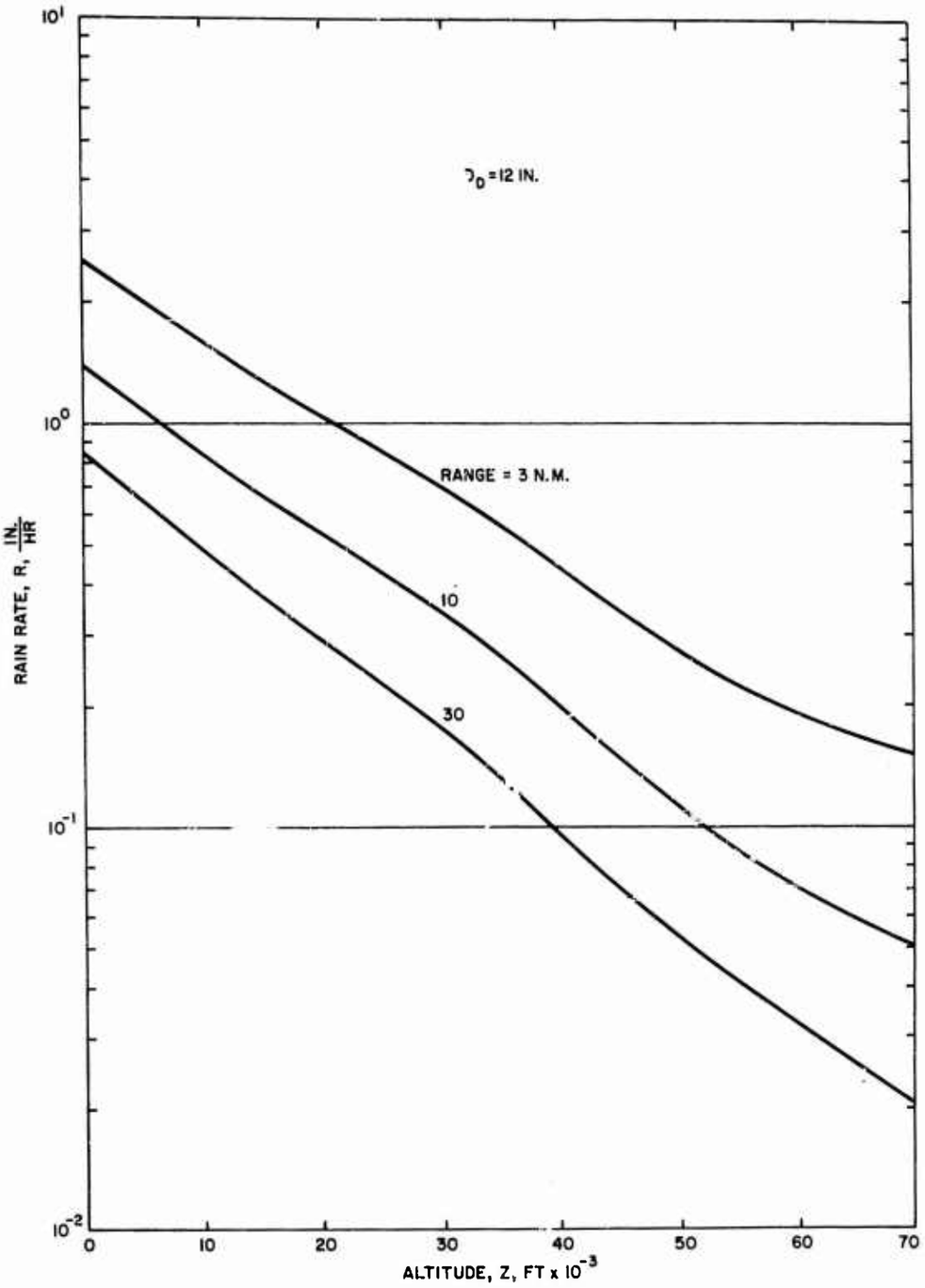

Figure 23. Allowable Rain Rate Versus Altitude for a 12-Inch Radome.

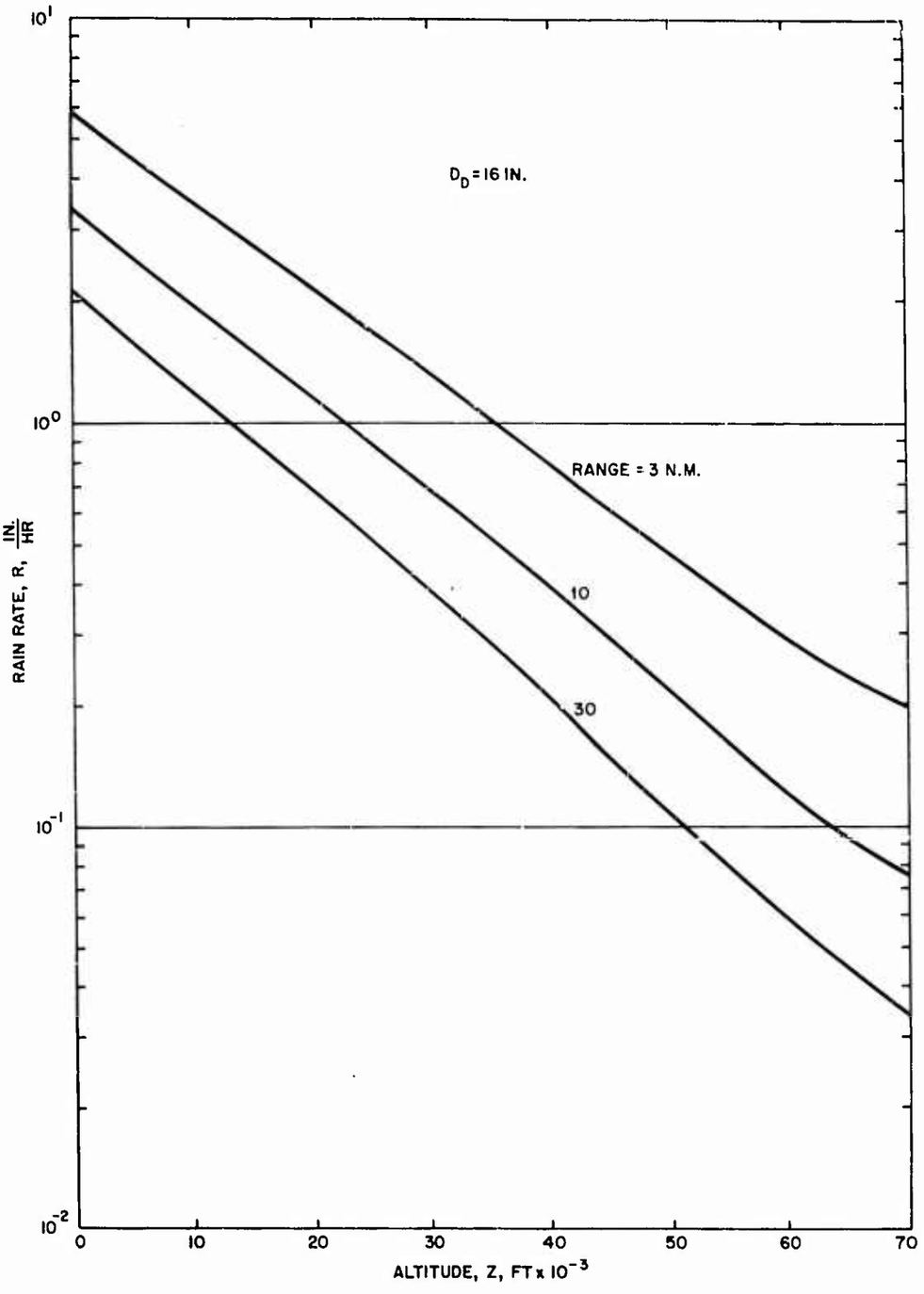

Figure 24. Allowable Rain Rate Versus Altitude for an 18-Inch Radome.

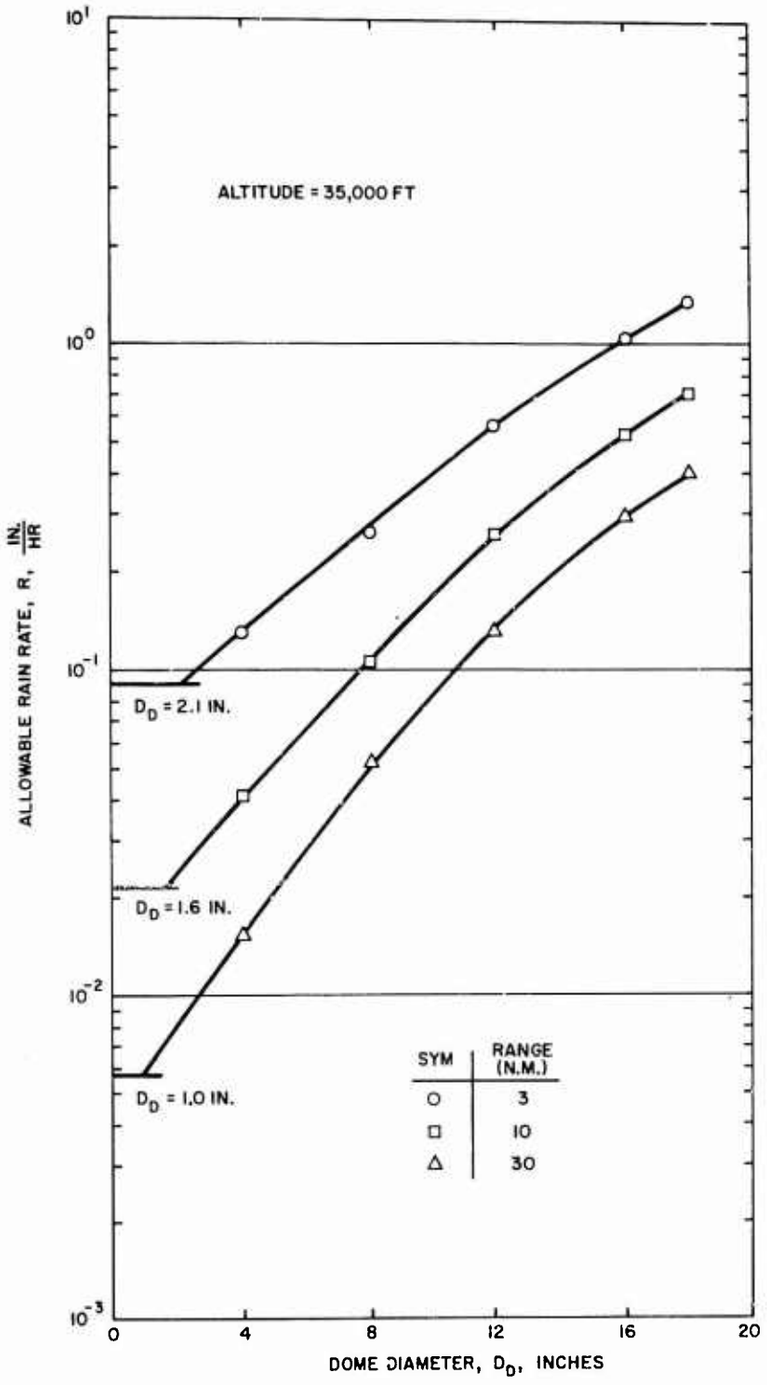

Figure 25. Allowable Rain Rate Versus Radome Diameter for a Flight at 35000 Feet.

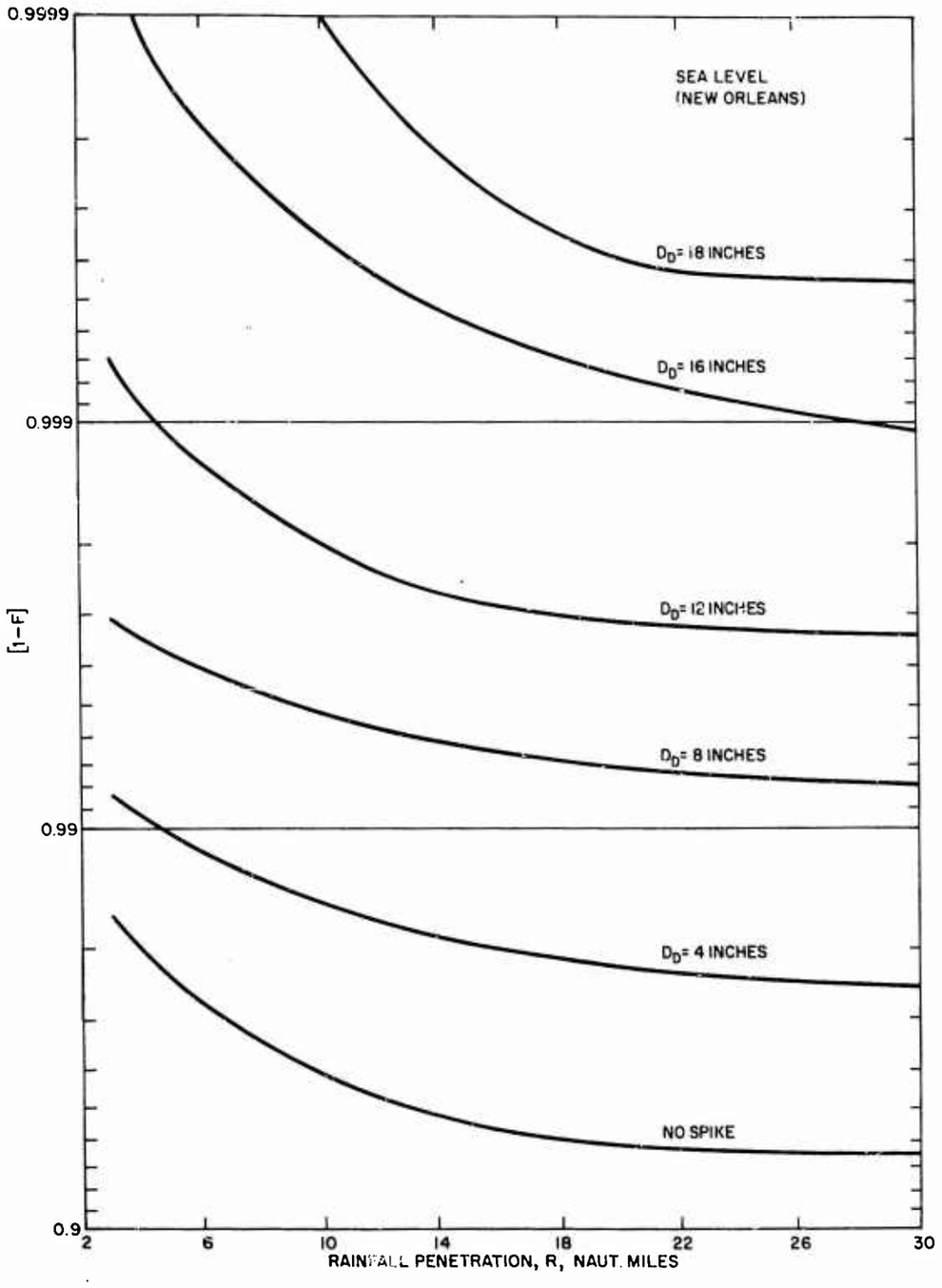

Figure 26. Fraction of Time During Year That a Missile Can Penetrate a Given Rainfall (New Orleans).

APPENDIX A

DIMENSIONAL ANALYSIS OF DROP BREAKUP BY AIRSTREAM IMPACT

In order to determine what the basic scaling parameters are, the simplest and most powerful tool available is dimensional analysis. This technique yields only the parameters which affect drop breakup and does not give any information as to the extent of the effect. The functional relation must be determined from an analysis of drop breakup or from an experiment.

In the drop breakup process, the most sensitive and easily measure parameter is the drop breakup time, t_b. In the analysis which follows this will be considered the dependent variable. There are eight additional parameters which may affect the breakup time. All of the variables are listed below with the appropriate units in terms of mass, M, length, L, and time, T:

Breakup time	t_b	T
Drop diameter	Do	L
Drop velocity	Vo	LT^{-1}
Drop density	ρ_d	ML^{-3}
Air density	ρ_a	ML^{-3}
Air viscosity	μ_a	$ML^{-1}T^{-1}$
Drop viscosity	μ_d	$ML^{-1}T^{-1}$
Drop surface tension	σ	MT^{-2}
Air sonic velocity	C	LT^{-1}

Any process may be described in terms of a series expansion:

$$t_b = a_1 D_o^{\alpha} V_o^{\beta} \rho_a^{\gamma} \rho_d^{\delta} \mu_a^{\epsilon_1} \mu_d^{\lambda} \sigma_d^{K} C^{\nu}$$

$$+ a_1 D_o^{2\alpha} V_o^{2\beta} \rho_d^{2\gamma} \rho_a^{2\delta} \mu_a^{2\epsilon_1} \mu_d^{2\lambda} \sigma_d^{2K} C^{2\nu} \qquad 4.1$$

$$+ - - - - -$$

The units of the left hand side of the equation are $M^oL^oT^1$. The terms on the right hand side of the equation may be grouped as:

$$L^{\alpha} \quad LT^{-1}^{\beta+\nu} \quad ML^{-3}^{\gamma+\delta} \quad ML^{-1}T^{-1}^{\epsilon+\lambda} \quad MT^{-2}^{K} \qquad 4.2$$

Equating the powers of the individual units yields three equations for the mass:

$$o = \gamma + \delta + \epsilon \lambda + K \qquad 4.3$$

length:

$$o = \alpha + \beta + \nu - 3\gamma - 3\delta - \epsilon - \lambda \qquad 4.4$$

and time:

$$1 = -\beta - \nu - \epsilon - \lambda - 2K \qquad 4.5$$

Naturally, an exact solution can not be obtained for each of the expenents since there are three equations and eight unknowns. However, three of the variables may be eliminated from the basic series expansion. The exponents α, β, and γ are chosen since in all physical analyses the drop diameter, velocity and local air density are found to be important independent variables. The exponents β and γ may be obtained directly from equations 4-5 and 4-3 as:

$$\beta = -1 - \nu - \epsilon - \lambda - 2K \qquad 4.6$$

$$\gamma = -\delta - \epsilon - \lambda - K \qquad 4.7$$

The expression for α is subsequently obtained as:

$$\alpha = 1 - \epsilon - \lambda - K \qquad 4.8$$

Substituting directly back into equation 4-1 yields:

$$t_b = a_1 \; D_o^{1-\epsilon-\lambda-K} \; V_o^{-1-\nu-\epsilon-\lambda-2K} \; \rho_a^{-\delta-\epsilon-\lambda-K}$$

$$\rho_d^{\delta} \; \mu_a^{\epsilon} \; \mu_d^{\lambda} \; \sigma^{K} \; C^{\nu} \qquad + a_2 \left(\qquad \right)^2 + \text{----} \qquad 4.9$$

This may be grouped as:

$$t_b = a_1 \frac{D_o}{V_o} \left(\frac{\rho_d}{\rho_a} \right)^{\delta} \left(\frac{\rho_a V_o D_o}{\mu_a} \right)^{-\lambda} \left(\frac{\rho_a V_o^2 D_o}{\sigma} \right)^{-K} \left(\frac{V}{C} \right)^{-\nu} \left(\frac{\rho_a V_o D_o}{\mu_d} \right)^{\epsilon}$$

$$+ a_2 \left(\qquad \right)^2 + \text{- - - -} \qquad 4.10$$

The drop breakup time may be normalized to yield the functional dependence:

$$\bar{t} = f(\bar{\rho},\ Re_a,\ W_e,\ M,\ Re_d) \qquad 4.11$$

where the normalized parameters are:

$$\bar{t} = \frac{t_b V_o}{D_o} \qquad 4.12$$

$$\bar{\rho} = \frac{\rho_d}{\rho_a} \qquad 4.13$$

$$Re_a = \frac{\rho_a V_o D_o}{\mu_a} \qquad 4.14$$

$$We = \frac{\rho_a V_o^2 D_o}{2\sigma} \qquad 4.15$$

$$M = \frac{V}{C} \qquad 4.16$$

$$Re_d = \frac{\rho_a V_o D_o}{\mu_w} \qquad 4.17$$

These are all of the non-dimensional parameters which can influence drop breakup. The terms Re, We and M are the Reynolds number, Weber number and Mach number respectively.

APPENDIX B

THE DISTRIBUTION OF DROP SIZES IN NATURAL RAIN

Any natural rainfall consists of drops of many different sizes. Casual observations reveal that the drops are on the whole smaller in light rain or drizzle and larger in heavy rains or thunderstorms. In either case there is a wide spread of drop sizes. In order to take these characteristics of rain into account, a quantitative model of natural rain is required. Although the use of a standard model is the only practical course, it should not be forgotten that individual rainstorms may vary considerably from this model

B.1 The (M-P)Distribution of Drop Sizes

The most commonly used empirical formula for the distribution of drop sizes in rain is due to Marshall and Palmer (1948). It is

$$N(d) = 0.08\, e^{-\lambda d} \ \text{cm}^4 \qquad \text{B.1}$$

where $N(d)\,\delta D$ is the number of drops per cm^3 having diameters in the range between d and $d + \delta d$.

The distribution of the liquid water content (LWC) among different drop sizes may be obtained by integration. The total (LWC) is

$$\frac{0.08\,\pi\,\rho_e}{6} \int_0^\infty d^3 e^{-\lambda d}\, dd \qquad \text{B.2}$$

$$= \frac{0.08\,\pi\,\rho_e}{6\lambda^4} \int_0^\infty t^3 e^{-t}\, dt$$

This reduces to

$$(LWC) = \frac{0.08\ \tau\ \rho_e}{\lambda^4} \qquad B.3$$

since the value of the integral is $\Gamma(4) = 6$.

The drops whose diameters are larger than d contain a fraction F (d) of this total water content where

$$F(d, \lambda) = \frac{\int_d^\infty d^3\, e^{-\lambda d}\, dd}{\int_0^\infty d^3\, e^{-\lambda d}\, dd} \qquad B.4$$

$$F(\lambda d) = \frac{1}{6} \int_{\lambda d}^\infty t^3\, e^{-t}\, dt \qquad B.5$$

The integral is an incomplete gamma function which is tabulated, for instance, in the NBS tables.

The value of λd corresponding to $F = 0.5$ defines a diameter d_o which splits the (LWC) in half. In other words half the (LWC) consists of drops with diameters smaller than d_o and the other half of drops with diameters larger than d_o. This median volume diameter will be used to characterize the mean drop size. It is related to λ by the formula

$$d_o = \frac{3.67}{\lambda} \qquad B.6$$

The variation of F with d/d_o is illustrated in Figure B.1.

B.2 Variation of the Mean Drop Diameter With Rain Rate

If $V_T(d)$ is the terminal velocity of a drop of diameter d, the rain rate is

$$R = \frac{\pi}{6} \int_0^\infty V_T(d)\, d^3\, e^{-\lambda d}\, dd \qquad B.7$$

Using an empirical formula for $V_T(d)$ Marshall and Palmer (1948) performed the integration and solved the resulting equation for λ in terms of R. With R' in mm/hr their result was

$$\lambda = 41\, R'^{-0.21} \text{ cm}^{-1} \qquad B.8$$

Using (B.6) and converting to R in in/hr we obtain the formula

$$d_o = 0.177\, R^{0.21} \text{ cm} \qquad B.9$$

which has been plotted in Figure B.2

B.3 Variation of Liquid Water Content with Rain Rate and Drop Size

The total liquid water content (mass/unit volume) of any rainfall may be computed by substituting the result (B.8) into the formula (B.3). With R in (in/hr) we obtain

$$(LWC) = 1.35\, R^{0.84} \text{ g/m}^3 \qquad B.10$$

The fraction of this consisting of drops whose diameter is greater than d may be obtained from the distribution curve shown in Figure B.1. This spreads out over a greater range of diameters as d_o increases with R. Figure B.3 illustrates the volumetric distribution of the (LWC) for a number of rain rates. In this figure the intercepts of the curves on the

d = 0 axis represent the total (LWC) as given by (B. 10) for each rain rate. For any other value of d the ordinate represent the fractional (LWC) for diameters greater than d.

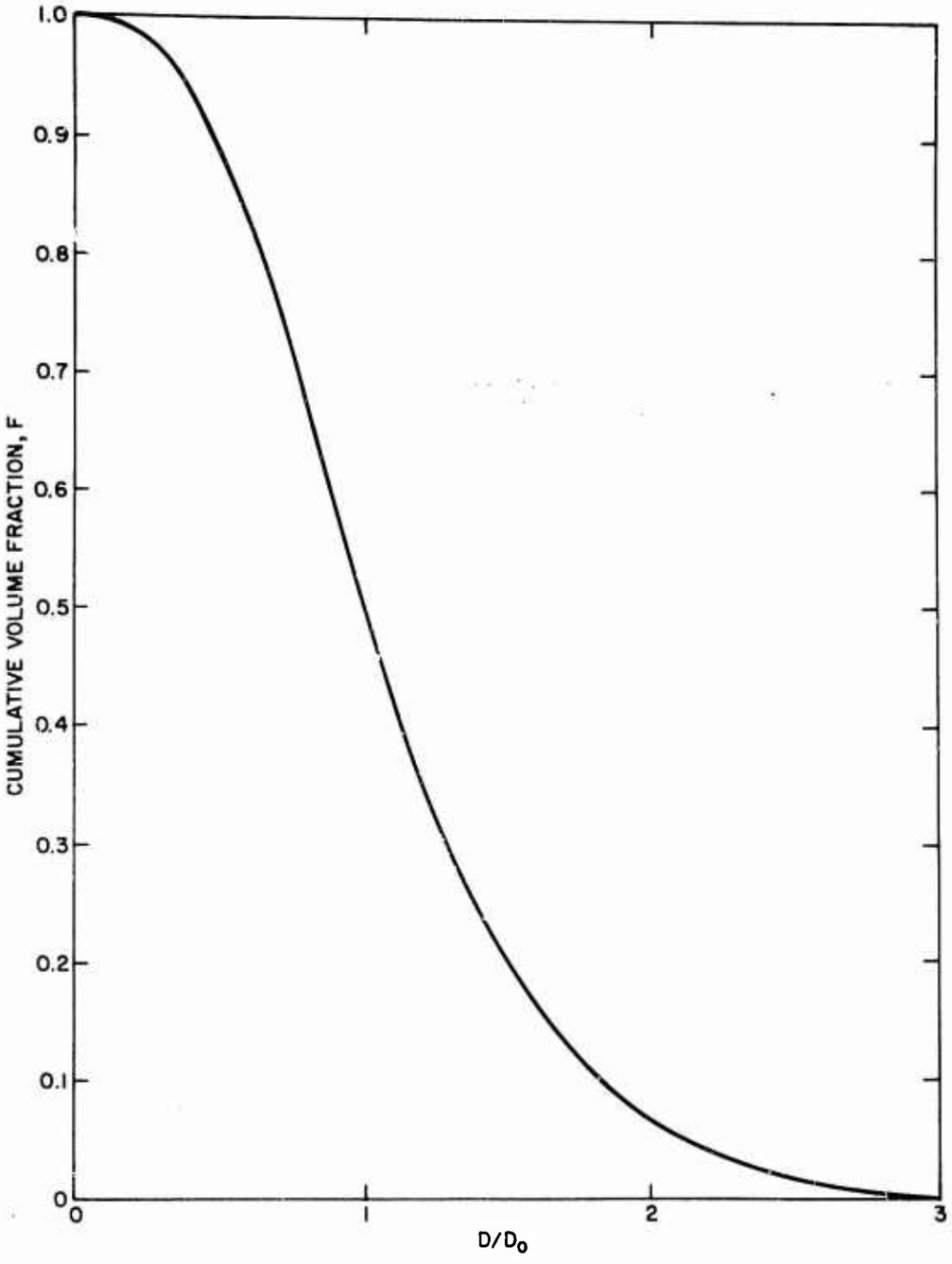

Figure B1. Cumulative Volume Distribution with Drop Size.

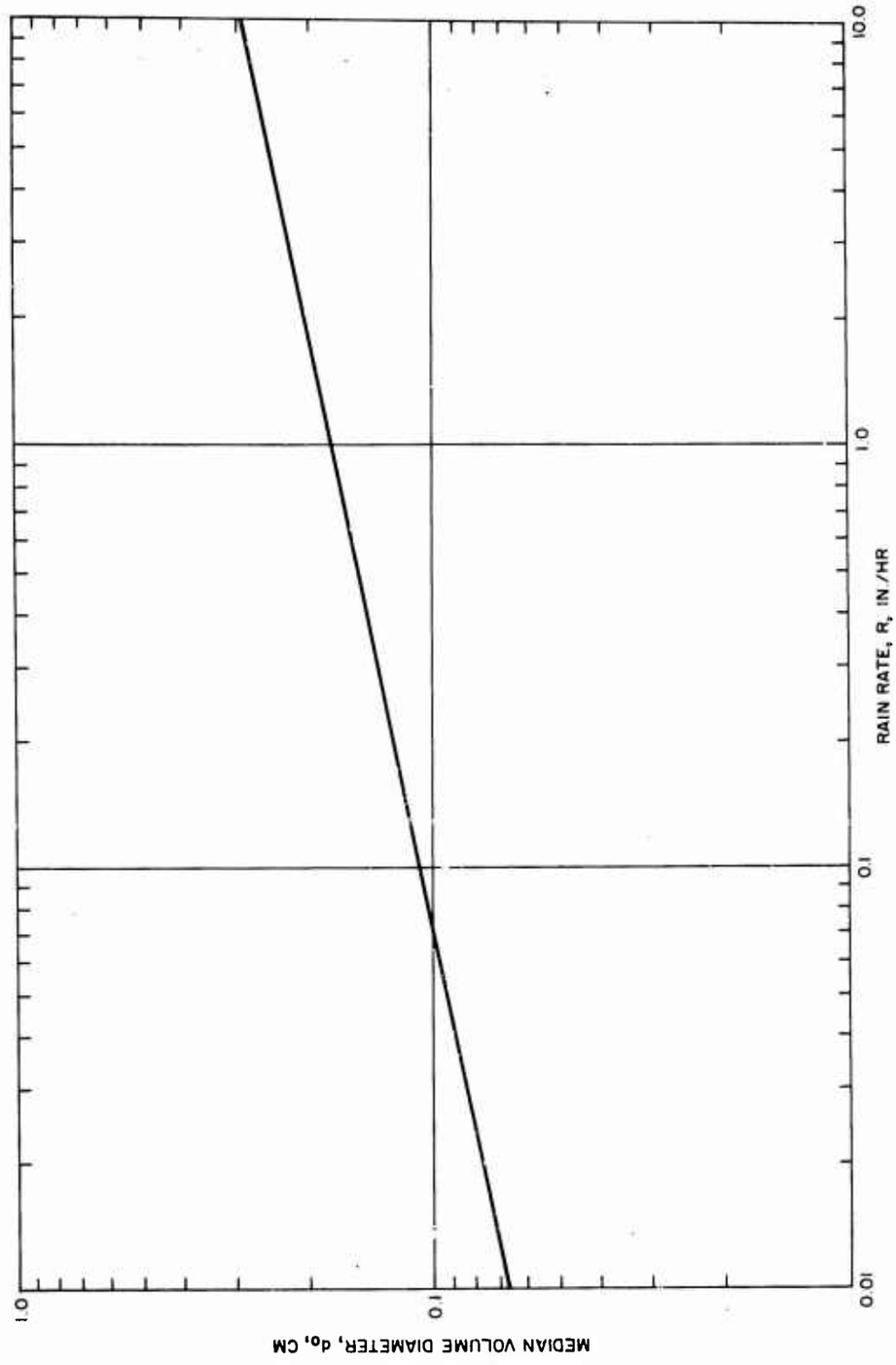

Figure B2. Median Volume Diameter Versus Rain Rate.

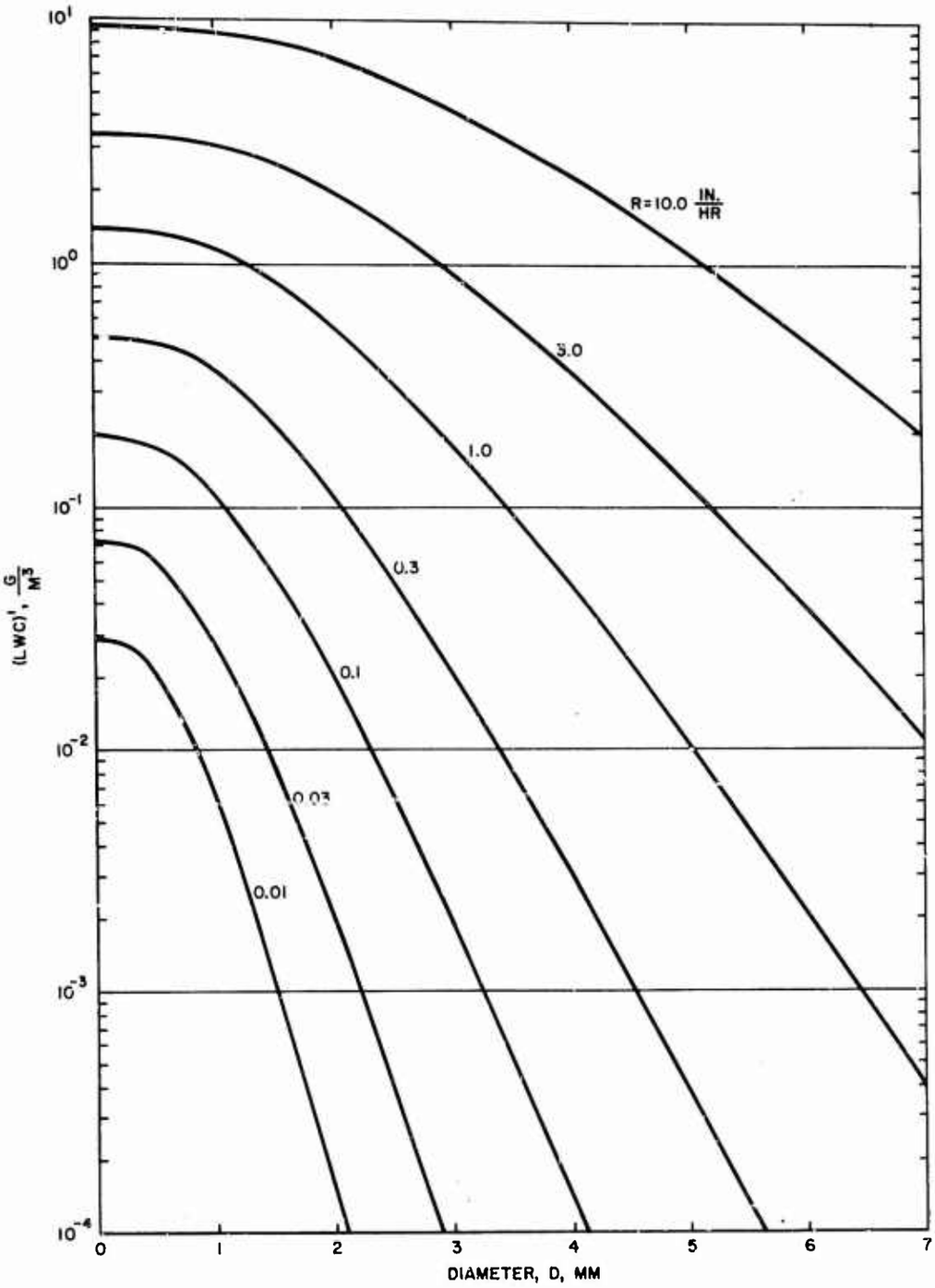

Figure B3. Liquid Water Content Versus Drop Diameter for Several Rain Rates.

MC 61-6-R3 MITHRAS, Inc., Cambridge, Mass. CONFIDENTIAL

RAIN EROSION ON SPIKE-PROTECTED SUPERSONIC RADOMES (Unclassified Title), Interim Engineering Report, Contract Nonr 3684(00), viii and 83 pages, April 1965.

This report describes a sled test and shock tube test program designed to assess the effectiveness of flow separation devices in providing rain erosion protection to missile radomes. In the sled test program models were run at supersonic speeds through heavy rain. Those models with the flow separating device sustained little or no damage whereas unprotected models were totally destroyed by rain erosion. In the shock tube, drop breakup was studied over a wide range of the basic scaling parameters. Correlation of the shock tube data with previous drop breakup theory and extension of this theory to the sled test conditions yields results in excellent agreement. These results are then used to predict flow separation configurations at other altitudes and velocities of interest. Based on the results of these two experimental programs and the follow-up analysis, it may be concluded that flow separation techniques are an effective solution to the problem of rain erosion at supersonic speeds.

1. Radomes
2. Rain Erosion
3. Spiked Bodies

I. MITHRAS, Inc. MC 61-6-R3
II. Nicholson, J. E.
III. Hill, J. A. F.

CONFIDENTIAL

MC 61-6-R3 MITHRAS, Inc., Cambridge, Mass. CONFIDENTIAL

RAIN EROSION ON SPIKE-PROTECTED SUPERSONIC RADOMES (Unclassified Title), Interim Engineering Report, Contract Nonr 3684(00), viii and 83 pages, April 1965.

This report describes a sled test and shock tube test program designed to assess the effectiveness of flow separation devices in providing rain erosion protection to missile radomes. In the sled test program models were run at supersonic speeds through heavy rain. Those models with the flow separating device sustained little or no damage whereas unprotected models were totally destroyed by rain erosion. In the shock tube, drop breakup was studied over a wide range of the basic scaling parameters. Correlation of the shock tube data with previous drop breakup theory and extension of this theory to the sled test conditions yields results in excellent agreement. These results are then used to predict flow separation configurations at other altitudes and velocities of interest. Based on the results of these two experimental programs and the follow-up analysis, it may be concluded that flow separation techniques are an effective solution to the problem of rain erosion at supersonic speeds.

1. Radomes
2. Rain Erosion
3. Spiked Bodies

I. MITHRAS, Inc. MC 61-6-R3
II. Nicholson, J. E.
III. Hill, J. A. F.

CONFIDENTIAL

MC 61-6-R3 MITHRAS, Inc., Cambridge, Mass. CONFIDENTIAL

RAIN EROSION ON SPIKE-PROTECTED SUPERSONIC RADOMES (Unclassified Title), Interim Engineering Report, Contract Nonr 3684(00), viii and 83 pages, April 1965.

This report describes a sled test and shock tube test program designed to assess the effectiveness of flow separation devices in providing rain erosion protection to missile radomes. In the sled test program models were run at supersonic speeds through heavy rain. Those models with the flow separating device sustained little or no damage whereas unprotected models were totally destroyed by rain erosion. In the shock tube, drop breakup was studied over a wide range of the basic scaling parameters. Correlation of the shock tube data with previous drop breakup theory and extension of this theory to the sled test conditions yields results in excellent agreement. These results are then used to predict flow separation configurations at other altitudes and velocities of interest. Based on the results of these two experimental programs and the follow-up analysis, it may be concluded that flow separation techniques are an effective solution to the problem of rain erosion at supersonic speeds.

1. Radomes
2. Rain Erosion
3. Spiked Bodies

I. MITHRAS, Inc. MC 61-6-R3
II. Nicholson, J. E.
III. Hill, J. A. F.

CONFIDENTIAL

MC 61-6-R3 MITHRAS, Inc., Cambridge, Mass. CONFIDENTIAL

RAIN EROSION ON SPIKE-PROTECTED SUPERSONIC RADOMES (Unclassified Title), Interim Engineering Report, Contract Nonr 3684(00), viii and 83 pages, April 1965.

This report describes a sled test and shock tube test program designed to assess the effectiveness of flow separation devices in providing rain erosion protection to missile radomes. In the sled test program models were run at supersonic speeds through heavy rain. Those models with the flow separating device sustained little or no damage whereas unprotected models were totally destroyed by rain erosion. In the shock tube, drop breakup was studied over a wide range of the basic scaling parameters. Correlation of the shock tube data with previous drop breakup theory and extension of this theory to the sled test conditions yields results in excellent agreement. These results are then used to predict flow separation configurations at other altitudes and velocities of interest. Based on the results of these two experimental programs and the follow-up analysis, it may be concluded that flow separation techniques are an effective solution to the problem of rain erosion at supersonic speeds.

1. Radomes
2. Rain Erosion
3. Spiked Bodies

I. MITHRAS, Inc. MC 61-6-R3
II. Nicholson, J. E.
III. Hill, J. A. F.

CONFIDENTIAL